Article

Probing one-dimensional systems via noise magnetometry with single spin qubits

RODRIGUEZ-NIEVA, Joaquin F., *et al*.

Abstract

The study of exotic one-dimensional states, particularly those at the edges of topological materials, demand new experimental probes that can access the interplay between charge and spin degrees of freedom. One potential approach is to use a single spin probe, such as a nitrogen vacancy center in diamond, which has recently emerged as a versatile tool to probe nanoscale systems in a noninvasive fashion. Here, we present a theory describing how noise magnetometry with spin probes can directly address several questions that have emerged in experimental studies of 1D systems, including those in topological materials. We show that by controlling the spin degree of freedom of the probe, it is possible to measure locally and independently local charge and spin correlations of 1D systems. Visualization of 1D edge states, as well as sampling correlations with wave-vector resolution can be achieved by tuning the probe-to-sample distance. Furthermore, temperature-dependent measurements of magnetic noise can clearly delineate the dominant scattering mechanism (impurities versus interactions)—this is of particular relevance to [...]

Reference

RODRIGUEZ-NIEVA, Joaquin F., *et al*. Probing one-dimensional systems via noise magnetometry with single spin qubits. *Physical Review. B, Condensed Matter*, 2018, vol. 98, no. 19, p. 195433

DOI : 10.1103/PhysRevB.98.195433

Editors' Suggestion

Probing one-dimensional systems via noise magnetometry with single spin qubits

Joaquin F. Rodriguez-Nieva,[1] Kartiek Agarwal,[2] Thierry Giamarchi,[3] Bertrand I. Halperin,[1] Mikhail D. Lukin,[1] and Eugene Demler[1]

[1]*Department of Physics, Harvard University, Cambridge, Massachusetts 02138, USA*
[2]*Department of Electrical Engineering, Princeton University, Princeton, New Jersey 08544, USA*
[3]*Department of Quantum Matter Physics, University of Geneva, Geneva 1211, Switzerland*

(Received 8 April 2018; published 21 November 2018)

The study of exotic one-dimensional states, particularly those at the edges of topological materials, demand new experimental probes that can access the interplay between charge and spin degrees of freedom. One potential approach is to use a single spin probe, such as a nitrogen vacancy center in diamond, which has recently emerged as a versatile tool to probe nanoscale systems in a noninvasive fashion. Here, we present a theory describing how noise magnetometry with spin probes can directly address several questions that have emerged in experimental studies of 1D systems, including those in topological materials. We show that by controlling the spin degree of freedom of the probe, it is possible to measure locally and independently local charge and spin correlations of 1D systems. Visualization of 1D edge states, as well as sampling correlations with wave-vector resolution can be achieved by tuning the probe-to-sample distance. Furthermore, temperature-dependent measurements of magnetic noise can clearly delineate the dominant scattering mechanism (impurities versus interactions)—this is of particular relevance to quantum spin Hall measurements where conductance quantization is not perfect. The possibility to probe both charge and spin excitations in a wide range of length scales opens new pathways to bridging the large gap between atomic scale resolution of scanning probes and global transport measurements.

DOI: 10.1103/PhysRevB.98.195433

I. INTRODUCTION

One-dimensional (1D) phases of matter exhibit a myriad of exotic phenomena including non-Fermi liquid behavior, charge-spin separation, and power-law scaling of charge and spin correlations [1–3]. Reinvigorated interest in such phases resulted from the recent realization of 1D edge states emerging in topological materials, for instance, quantum spin Hall states [4–7]. The design of new experimental probes to access these interesting and exotic states is highly desirable but equally demanding. For instance, because in many cases 1D states live at the edges of higher dimensional systems, several experimental probes are limited by the negligibly small scattering cross section, e.g., neutron or light scattering. Furthermore, probes that can bridge the large length-scale gap between atomic scale resolution of scanning tunneling probes and global transport measurement are on high demand, in particular to obtain correlations with wave-vector resolution. Accessing physics at the nanometer scale, however, impose stringent requirements on probe size.

Motivated by the rapid progress in magnetic noise spectroscopy with single spin qubits, such as nitrogen vacancy (NV) centers in diamond [8–13], here we outline pathways to exploit single spin probes to access 1D physics in a broad range of 1D systems, including those emerging in topological materials. Spin probes harness the fluctuating magnetic field induced by quantum and thermal fluctuations of 1D charged and spin modes. By measuring the spin relaxation time T_1 as a function of experimentally tunable parameters, e.g., temperature (T), probe-to-sample distance (R), and spin probe polarization, 1D correlations can be obtained. There are several key advantages of single spin probes. Because of their atomic size, spin probes enable measurements with nanometer resolution, much smaller than the micron scales achievable via NMR [14], and makes the measurement insensitive to boundary effects, such as the contacts. This feature also grants access to spin fluctuations, which can only be detected at nanometer scale proximity due to short-range dipole-dipole interaction and which have been elusive with a (superconducting quantum interference device) SQUID [15]. In addition, because the electromagnetic coupling between the probe and the sample decays as a power law, different from the exponential decay of scanning tunneling currents, single spin probes can access a broader range of length scales, from few to a hundred nanometers. Another interesting feature is that, because spin probes do not require driving fields, i.e., they are driven by charge and spin fluctuations in the sample, they are minimally invasive.

The success of this technique in the study of excitations in higher-dimensional materials, such as metallic surfaces [10] and ferromagnets [11–13], combined with theoretical proposals to measure electron viscosity in the hydrodynamic regime [16], forecasts grand new vistas in 1D. Interestingly, as compared to larger dimensional systems, we find that the noise behavior in 1D systems features two fundamental differences which can be rendered into practical advantages. First, it was shown that magnetic fluctuations emerging from metallic surfaces are dominated by transverse charge currents, thus making noise originating from longitudinal currents (i.e., charged modes) and spin fluctuations inaccessible [16]. The absence of transverse charge currents in 1D grants access to charge and spin-induced fluctuations simultaneously when the

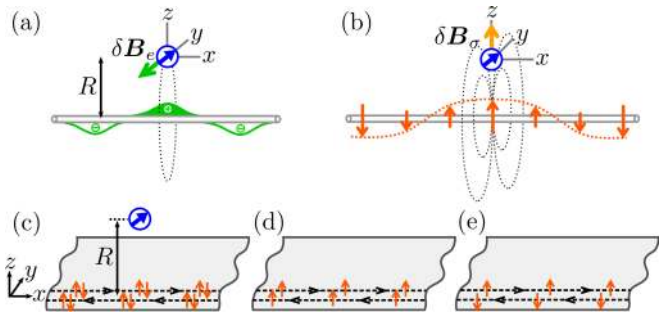

FIG. 1. Separating charge and spin fluctuations of one-dimensional (1D) systems using single spin qubits. For 1D systems, the spin probe (blue spin) can *independently* probe (a) charge fluctuations and (b) spin fluctuations in the quantum wire. Charge fluctuations induce magnetic noise $\delta \boldsymbol{B}_e$ in the azimuthal direction ($\hat{y}$), whereas spin fluctuations induce magnetic noise $\delta \boldsymbol{B}_\sigma$ primarily in the radial ($\hat{z}$) and azimuthal ($\hat{y}$) directions. The spin degree of freedom of the probe can be used to filter the charge fluctuations from the spin fluctuations. To understand how the internal structure of 1D states affects noise, here we use three prototypical examples: (c) two counterpropagating channels with an SU(2) degree of freedom; (d) a spin-polarized edge state comprised of right and left movers with equal spin polarization; (e) nonchiral helical edge states comprised of right and left movers with opposite spin polarizations.

probe is sufficiently close to the sample. Second, not only is it possible to access both charge and spin excitations but also *separate* them, even when they are comparable. As shown in Figs. 1(a) and 1(b), this feature arises because of the spin degree of freedom of the probe, which allows to measure B-field in different directions: whereas charge fluctuations induce magnetic fields in the azimuthal direction $\hat{\theta}$, spin fluctuations induce magnetic fields in all spatial directions (the radial and azimuthal components dominate at long wavelengths, see below). Since the relaxation time of a spin probe is determined only by magnetic field fluctuations perpendicular to the orientation of the spin probe, we see that charge-induced noise can be filtered from spin-induced noise by aligning the spin probe with the azimuthal direction, i.e., the probe acting as a vector magnetometer [17]. Therefore spin probes represent an important departure, for instance, from scanning tunneling probes which cannot separate charge and spin excitations [18–22]. For example, even if the tunneling tip is spin-polarized, this technique still requires tunneling of electrons into the sample and, as such, does not work in insulating materials with spin excitations.

Besides polarization direction, other experimentally tunable parameters are available to access different features of 1D states, such as scattering and transport. For instance, by tuning the probe-to-sample distance R and scanning magnetic noise at different length scales, it is possible to sample correlations with wave-vector resolution and diagnose transport behavior, i.e., whether charge and spin density waves propagate ballistically or are pinned by disorder. Furthermore, we find that scattering is the key factor leading to non-universal power law behavior of noise versus T; the specific T dependence hints at the nature of backscattering, i.e., whether it is single-particle or interaction-assisted.

We also stress that T_1 measurements is one of the many available experimental protocols to measure correlations in interacting systems. A variety of dynamic protocols, such as relaxometry in the presence of driving (dressed methods) or using special pulse sequences, are discussed in Ref. [23].

Turning our discussion to specific 1D models, we first note that, at the sub-THz frequencies characteristic of spin probes in current experimental setups, a good starting point to describe general 1D systems is the Luttinger liquid (LL) theory [24–26]. To capture the key aspects of magnetic noise measurements, we exploit minimal models that qualitatively describe the effects of scattering, interactions, and internal structure of 1D states. Because we need at least two 1D channels to describe scattering, here we mainly focus on nonchiral, two-channel systems such that one channel is right-moving and the other is left-moving.

To aggregate the internal structure of 1D states into our discussion, we consider three minimal models. First, we consider that each channel has an SU(2) degree of freedom [Fig. 1(c)], which is the most usual case describing quantum wires or metallic nanotubes. Second, we consider a spin-polarized LL [27,28] in which excitations are comprised of left-moving and right-moving modes with equal spin polarization [Fig. 1(d)]. Third, and motivated by the recent realization quantum spin Hall states, we consider a pair of counterpropagating helical edge state. Contrary to the previous case, the right-moving and left-moving excitations have opposite spin polarizations [Fig. 1(e)]. The helical state differs from the SU(2) and spin-polarized states in several important ways. In particular, when time-reversal symmetry is present, carriers cannot be backscattered by disorder as this would require a spin flip [29]; as such, backscattering needs to be assisted by interactions [30–35]. Below we describe how the interplay between scattering, interactions and internal structure of carriers affect the noise spectrum.

The outline of the present work is as follows. In Sec. II, we present the theory of magnetic noise spectroscopy and, in particular, how T_1 can be computed from charge and spin density correlations of the 1D system. In Sec. III, we focus on the magnetic noise behavior of clean wires described within the LL theory, and describe how it varies as a function of experimentally tunable parameters, in particular probe-to-sample distance, temperature and interactions strength. In Sec. IV, we introduce weak, dense disorder (Gaussian disorder) and describe how the noise behavior is qualitatively modified from the LL behavior. In Sec. V, we introduce sparse, strong impurities (Poisson disorder) and describe the effect on magnetic noise. In Sec. VI, we discuss scenarios that go beyond our minimal two-channel model and, in Sec. VII, we summarize the main results.

II. RELAXATION TIME MEASUREMENT: GENERAL FORMALISM

We begin by describing a general formalism that allows to relate the relaxation time T_1 with charge and spin density correlations of general 1D systems. With this objective in mind, we first consider a generic 1D system with charge and spin dynamics governed by the action $\mathcal{S}_{1D}$ (below we introduce specific microscopic models). The coupled dynamics of the

wire and the electromagnetic field is described by the action

$$\mathcal{S} = \mathcal{S}_{1D} - \iint dt d\boldsymbol{r}[F^{\mu\nu}F_{\mu\nu}/4\mu_0 + A_\mu J^\mu], \quad (1)$$

where we use standard 4-vector covariant notation, $F^{\mu\nu}$ denotes $F^{\mu\nu} = \partial^\mu A^\nu - \partial^\nu A^\mu$, A^μ is the vector potential, μ_0 is the vacuum permeability, and coordinates are in three-dimensional space, $\boldsymbol{r} = (x, y, z)$. Assuming wire coordinates to be $\boldsymbol{r} = (x, 0, 0)$, charge and spin density fluctuations in the wire act as sources of electromagnetic field via the term $J^\mu = J_e^\mu + J_\sigma^\mu$:

$$J_e^\mu = e[c\rho_e(x,t), 0, 0, j_e(x,t)]\delta(y)\delta(z),$$
$$J_\sigma^\mu = (0, \nabla \times \boldsymbol{m}), \quad \boldsymbol{m} = g_\sigma \mu_B \sum_{i=x,y,z} \rho_i(x,t)\delta(y)\delta(z)\hat{\boldsymbol{e}}_i, \quad (2)$$

where c is the speed of light, μ_B the Bohr magneton, and g_σ the g factor of the spin modes in the wire. For a 1D system, the carrier density ρ_e and the current j_e are related by the continuity equation, $\partial_t \rho_e = -\partial_x j_e$. For systems with a free SU(2) spin degree of freedom, any of the spin components $\rho_{x,y,z}(x,t)$ can fluctuate independently; for spin-polarized systems, we assume that fluctuations are given by $\rho_i = \rho_\sigma \hat{\boldsymbol{n}}_i$, where $\hat{\boldsymbol{n}}_i$ is the direction of polarization.

In thermal equilibrium, Eq. (1) combined with the sources in Eq. (2) give rise to fluctuations in electric and magnetic field induced by ρ_e and ρ_σ in the quantum wire, as well as vacuum electromagnetic fluctuations. A spin probe at position $\boldsymbol{r}$ is sensitive to fluctuations in magnetic field $\delta\boldsymbol{B}(\boldsymbol{r}, t)$ [36–40]. For concreteness, here we consider a spin-1/2 probe with an intrinsic level splitting $\hbar\omega$. The spin dynamics is governed by the time-dependent Hamiltonian $\mathcal{H}_{\text{spin}} = (\hbar\omega/2)\hat{\boldsymbol{n}}_p \cdot \boldsymbol{\sigma} + g_s\mu_B[\boldsymbol{\sigma} \cdot \delta\boldsymbol{B}(\boldsymbol{r}, t)]$, where g_s is the g factor of the probe. The direction of the intrinsic polarizing field, $\hat{\boldsymbol{n}}_p$, is determined by the nature of the spin probe. For instance, in the case of NV centers in diamond, the NV defect is a C_{3v} defect with a triplet ground state (the degeneracy is lifted by spin-spin interaction of the orbital levels). In this case, $\hat{\boldsymbol{n}}_p$ is the axis of the NV defect in the diamond lattice. Without loss of generality, we align $\hat{\boldsymbol{n}}_p$ with the $\hat{\boldsymbol{z}}$ axis. The relaxation time can be calculated using Fermi Golden's rule, which yields

$$\frac{1}{T_1} = \frac{(g_s\mu_B)^2}{2\hbar^2}\int_{-\infty}^{\infty} dt e^{i\omega t}\langle\{\delta B^+(\boldsymbol{r}, t), \delta B^-(\boldsymbol{r}, 0)\}\rangle, \quad (3)$$

and quantifies the amplitude of magnetic fluctuations, i.e., the magnetic noise in units of sec^{-1}, at the position of the probe [see derivation in Appendix A]. Importantly, a spin probe with level splitting $\hbar\omega$ only couples to magnetic modes oscillating at frequency ω. In Eq. (3), $\delta B^\pm$ denotes $\delta B^\pm = \delta B^x \pm i\delta B^y$, $\{,\}$ denotes anticommutation, and $\langle . \rangle$ denotes statistical average on the canonical ensemble at temperature T. Further, we assume that the probe is far away from any metallic contact which can produce background noise. Given that typical band gaps in the bulk of topological and/or substrate materials is much larger than typical level splittings $\hbar\omega$ of the spin qubit, we do not expect such sources to produce sizable magnetic noise.

The calculation of the magnetic noise, Eq. (3), for a generic 1D system can be simplified under several legitimate assumptions. First, we assume translational invariance in the direction of the wire ($\hat{\boldsymbol{x}}$), which is descriptive of the long wavelength behavior expected to occur at the characteristic sub-THz frequencies. Translational-symmetry breaking effects, e.g., disorder or commensurability, can be accounted for in terms of self-energy corrections, as will be described below. Second, we assume quasistatic dynamics of the electromagnetic field, such that δB_i tracks ρ_e and $\rho_{x,y,z}$ without any retardation effects; this is generally valid in solid state systems because excitations propagate with velocities much smaller than c. Under these assumptions, the 1D charge density, ρ_e, and the spin densities, $\rho_{x,y,z}$, give rise to four orthogonal electromagnetic modes:

$$\delta\boldsymbol{B}(\boldsymbol{r}, t) = \frac{1}{\sqrt{L}}\sum_{q\omega m} \boldsymbol{H}_m(q, y, z, \omega)e^{i(qx-\omega t)}\rho_m(q, \omega), \quad (4)$$

where $\boldsymbol{H}_m$ is the magnetic eigenfunction associated with each mode $m = e, x, y, z$, and L is the length of the wire. Vacuum electromagnetic fluctuations also contribute to Eq. (4), but we expect these to be negligibly small compared to wire-induced fluctuations.

The solution of Maxwell's equation for charge and spin fluctuations is discussed in Appendix B. To illustrate the qualitative behavior, here we present a more intuitive approach in the simple geometry of Fig. 1(c) in which the probe is at $\boldsymbol{r} = (0, 0, R)$. Focusing first on charge fluctuations and assuming quasistatic behavior, we can calculate magnetic field via Biot-Savart's law, $\delta\boldsymbol{B}_e(t) = \frac{\mu_0 e}{4\pi}\int_{-\infty}^{\infty} dx' j_e(x', t)\frac{\hat{\boldsymbol{x}}\times(\boldsymbol{r}'-\boldsymbol{r})}{|\boldsymbol{r}'-\boldsymbol{r}|^3}$, with $\boldsymbol{r}' = (x', 0, 0)$ wire coordinates. Currents can be related to charge density via the continuity equation $\partial_t\rho = -\partial_x j$, i.e., $j(x,t) = (\omega/q)\rho_m(q,\omega)e^{i(qx-\omega t)}/\sqrt{L}$, so that $\delta\boldsymbol{B}_e(t)$ can be rewritten as $\delta\boldsymbol{B}_e(t) = \frac{\mu_0 e\omega\rho_e(q,\omega)}{4\pi\sqrt{L}}\int_{-\infty}^{\infty} dx' \frac{Re^{iqx'}}{q(R^2+x'^2)^{3/2}}\hat{\boldsymbol{y}}$ [here we defined $\rho(x) = \frac{1}{\sqrt{L}}\sum_q \rho(q)e^{iqx}$]. Integration in x' leads to magnetic field written in the form (4) with

$$\boldsymbol{H}_e(q, 0, R, \omega) = -\frac{\mu_0 e}{2\pi}\begin{pmatrix} 0 \\ \omega K_1(qR) \\ 0 \end{pmatrix}, \quad (5)$$

where $K_n(x)$ is the nth modified Bessel function of the second kind. Naturally, $\delta\boldsymbol{B}_e$ points in the azimuthal direction. We also note that $K_n(x)$ is polynomial in x for $x \lesssim 1$, $K_n(x) \propto 1/x^n$, but decays exponentially for $x \gtrsim 1$, $K_n(x) \propto e^{-x}/\sqrt{x}$. Physically, such transition at $qR \approx 1$ occurs because for large R there is a negligible signal due to wave interference of the electromagnetic field.

Contrary to charge density, the spin-induced electromagnetic field has components in all three spatial directions, but the radial and axial components (with respect to the axis of the wire) dominate in the long-wavelength limit, $qR \ll 1$. The components of $\boldsymbol{H}_m$ are given by

$$\boldsymbol{H}_x(q, 0, R, \omega) = \frac{\mu_0 g_\sigma \mu_B q^2}{4\pi}\begin{pmatrix} -2K_0(qR) \\ 0 \\ 2iK_1(qR) \end{pmatrix},$$
$$\boldsymbol{H}_y(q, 0, R, \omega) = \frac{\mu_0 g_\sigma \mu_B q^2}{4\pi}\begin{pmatrix} 0 \\ K_0(qR) + K_2(qR) \\ 0 \end{pmatrix},$$
$$\boldsymbol{H}_z(q, 0, R, \omega) = \frac{\mu_0 g_\sigma \mu_B q^2}{4\pi}\begin{pmatrix} 2iK_1(qR) \\ 0 \\ K_0(qR) - K_2(qR) \end{pmatrix}. \quad (6)$$

As such, $\delta \boldsymbol{B}_e$ and $\delta \boldsymbol{B}_\sigma$ can be separated by exploiting the probe polarization direction. The spin-induced field exhibits the same power law to exponential transition occurring at $qR \approx 1$ as in the charge-induced field.

To measure correlations of the charge degrees of freedom, we assume that the spin qubit is aligned in direction $\hat{z}$, see Fig. 1. To measure correlations of the spin degrees of freedom, we assume that the spin qubit is aligned in the $\hat{y}$ direction. After a series of uneventful steps described in Appendix A, in particular replacing Eq. (4) into Eq. (3), and expressing density fluctuation in terms of dissipation in the wire, we find that $1/T_1$ induced by charge and spin modes is given by

$$\frac{1}{T_{1,m}} = \left(\frac{g_s \mu_B}{\hbar}\right)^2 \coth\left(\frac{\hbar\omega}{2k_B T}\right) \frac{1}{L} \sum_q F_m(q, y, z, \omega) \times \mathrm{Im}\left[\mathcal{C}^R_{\rho_m \rho_m}(q, \omega)\right], \quad m = e, \sigma. \tag{7}$$

Here, $\mathcal{C}^R_{\rho_m \rho_m}(q, \omega)$ is the short-hand notation for the retarded density-density correlation function, $\mathcal{C}^R_{AB}(q, \omega) = -i \int_0^\infty dt \langle [A(t), B(0)] \rangle e^{i\omega t}$. The factors $F_m(q, y, z, \omega)$ quantify the electromagnetic coupling between the wire and the probe and depends on the direction of intrinsic polarization of the probe. For charge modes, it is given by $F_e(q, y, z, \omega) = |H_e^y(q, y, z, \omega)|^2$ when the probe is polarized in the $\hat{x}$ and $\hat{z}$ directions, and 0 otherwise. For spin noise, we aggregate the three components of spin fluctuations $\rho_{x,y,z}$ into a single term $1/T_{1,\sigma}$, and quote the results in the case $qR \lesssim 1$ (the general solution is discussed in Appendix A). For the SU(2) case with the spin qubit aligned in the $\hat{y}$ direction, $F_\sigma(q, y, z, \omega) \approx |H_z^z(q, y, z, \omega)|^2$ in Eq. (6), where we assumed that $\langle \rho_x \rho_x \rangle = \langle \rho_y \rho_y \rangle = \langle \rho_z \rho_z \rangle$, and that fluctuations in each spin component are independent. For spin-polarized states, we find and $F_\sigma(q, y, z, \omega) = |H_z^z(q, y, z, \omega)|^2 \sin^2\theta \cos^2\varphi$, where θ and φ parametrize the spin polarization of the sample, $\hat{\boldsymbol{n}} = (\cos\theta, \sin\theta \sin\varphi, \sin\theta \cos\varphi)$.

Interestingly, we note that Eq. (7) resembles the standard $1/T_1$ equation for NMR relaxation, except for the q and $\boldsymbol{r}$ dependent form factors. Further, in the case of charge fluctuations, noise measurements can be related to conductivity $\sigma(q, \omega)$ measurements at finite q and ω. In particular, by using the continuity equation $\omega \rho_e = q j_e$ and the definition $\sigma(q, \omega) = \langle j_q \bar{j}_q \rangle / i\omega$, Eq. (7) can be expressed as $1/T_{1,e} \propto \sum_q q^2 F(q, y, z, \omega) \mathrm{Re}[\sigma(q, \omega)]/\omega$.

Equation (7) captures the essence of the noise measurement by making the connection between T_1 and charge and spin density correlations in a generic 1D system. In particular, by tuning $R = \sqrt{y^2 + z^2}$, it is possible to sample fluctuations at different wave vectors q by changing the weight of the form factor $F_m(q, y, z, \omega)$. For instance, for $q \lesssim 1/R$, the form factors as a function of q behaves as $[q^2 F_e(q)] \sim 1$ for charge noise, and $[q^2 F_\sigma(q)] \sim q^2$ for spin noise, i.e., there is finite sampling of charge and spin fluctuations for all modes with wave vectors $q \lesssim 1/R$. For $q \gtrsim 1/R$, the form factor for charge noise behaves as $[q^2 F_e(q)] \sim q e^{-2qR}$, and for spin noise as $[q^2 F_\sigma(q)] \sim q^5 e^{-2qR}$. As such, there is a sharp cutoff in the sampling of fluctuations occurring at $q \sim 1/R$ introduced by the exponential q dependence of $F_m(q, y, z, \omega)$. Such wave-vector selectivity allows to study correlations with wave-vector resolution and which, as we will see, is a useful feature in the study of disordered systems.

We now proceed to specify microscopic 1D models from which the density correlation $\mathcal{C}^R_{\rho_m \rho_m}(q, \omega)$ can be computed explicitly. This is the objective of the next two sections.

III. NOISE FROM LUTTINGER LIQUIDS

To capture the microscopics of the wire, we use the bosonization description for 1D electronic systems [3]. This framework is ideally suited for our purposes given the typically small sub-THz probing frequencies, much smaller than typical bandwidths in electronic systems, and its ability to describe 1D states of different flavors. Further, it provides a good starting point to describe more complex scenarios such as disordered wires. We set the stage by discussing magnetic noise in ballistic 1D channels with an SU(2) degree of freedom. Afterwards, we describe noise in clean spin-polarized and helical channels and point out the differences with the SU(2) case.

A. Case I: SU(2) channels

The motion of spinful fermions in a 1D channel can be described with a bosonic 1D action with separated charge and spin degrees of freedom:

$$\mathcal{S}_{1D} = \iint dt dx \sum_{m=e,\sigma} [\, i \Pi_m \partial_t \phi_m - \mathcal{H}_m(\phi_m, \Pi_m)]. \tag{8}$$

The bosonized degrees of freedom, Π_m and ϕ_m, are canonically conjugate, $[\phi_m(x), \Pi_{m'}(x')] = i\delta_{mm'}\delta(x - x')$, and describe charge ($m = e$) and spin ($m = \sigma$) excitations. In the absence of scattering, dynamics is governed by a quadratic Hamiltonian of the form

$$\mathcal{H}_m(\phi_m, \Pi_m) = \frac{\hbar v_F}{2\pi} [(\pi \Pi_m)^2 + (\partial_x \phi_m)^2], \quad m = e, \sigma, \tag{9}$$

where v_F is the Fermi velocity. In the long wavelength limit, charge and spin density are related to the bosonic degrees of freedom via $\rho_{e,\sigma} = -\sqrt{2}\partial_x \phi_{e,\sigma}/\pi$. This linear mapping $(\rho_e, \rho_\sigma) \leftrightarrow (\phi_m, \Pi_m)$ is valid up to spatially oscillating terms with wave vector k_F, the Fermi wave vector. Because these rapidly oscillating density terms produce negligibly small evanescent magnetic fields at distances larger than a few atomic sites, we do not explicitly keep track of them. Further, because of SU(2) symmetry, spin fluctuations in all spatial directions are equal, $\mathcal{C}^R_{\rho_m \rho_m}(q, \omega) = \mathcal{C}^R_{\rho_\sigma \rho_\sigma}(q, \omega)$. Importantly, we note that Eq. (9) does not include Coulomb interactions. This avoids double-counting the Coulomb potential which is mediated by $A^\mu(\boldsymbol{r}, t)$ already included in the full action in Eq. (1).

Having established the microscopic model via Eqs. (1), (8), and (9), and the mapping $(\rho_e, \rho_\sigma) \leftrightarrow (\phi_m, \Pi_m)$, we now proceed to calculate $\mathcal{C}^R_{\rho_m \rho_m}(q, \omega)$ in Eq. (7). The linear nature of the mapping $(\rho_e, \rho_\sigma) \leftrightarrow (\phi_m, \Pi_m)$ simplifies calculations significantly. First, because $A^\mu(\boldsymbol{r}, t)$ couples linearly to ϕ and Π in Eq. (1), and the action is quadratic in $A^\mu(\boldsymbol{r}, t)$, we can integrate exactly the electromagnetic modes coupled to charge/spin densities and incorporate them into an effective Hamiltonian $\langle \mathcal{H}_m \rangle_A$ with renormalized parameters. Secondly,

because of the linear mapping $(\rho_e, \rho_\sigma) \leftrightarrow (\phi_m, \Pi_m)$, charge and spin density correlators are two-point correlation functions in the bosonic field, which are straightforward to calculate for quadratic Hamiltonians.

Using these two simplifications, we proceed to obtain $\mathcal{C}^{\mathrm{R}}_{\rho_m\rho_m}(q,\omega)$. Because of translational invariance in the $\hat{\boldsymbol{x}}$ direction, it is convenient to rewrite the bosonic fields in Fourier space, $\phi_m(x) = \frac{1}{\sqrt{L}}\sum_q \phi_m(q)e^{iqx}$ and $\Pi_m(x) = \frac{1}{\sqrt{L}}\sum_q \Pi_m(q)e^{iqx}$. Spatial integration of the electromagnetic degrees of freedom result in the effective Hamiltonian

$$\langle \mathcal{H}_m\rangle_A(\phi_m,\Pi_m) = \frac{\hbar v_m}{2\pi}\left[\mathcal{K}_m[\pi\Pi_m(q)]^2 + q^2\phi_m^2(q)/\mathcal{K}_m\right], \tag{10}$$

where the parameters v_m and $\mathcal{K}_m$ are the renormalized velocity and the Luttinger parameter in the charge $(m = e)$ and spin sectors $(m = \sigma)$. The value of $\mathcal{K}_m$ quantifies the charge $(m = e)$ and spin $(m = \sigma)$ compressibility. In particular, at small q, renormalization of the Luttinger parameters in the charge sector is governed by Coulomb energy induced by the charge density $(= \frac{\epsilon_0}{2}\int d\boldsymbol{r}|\delta \boldsymbol{E}_e(\boldsymbol{r},t)|^2)$, which leads to a $\ln(1/qr_*)$ dependence:

$$\begin{aligned} v_e &= v_{\mathrm{F}}\sqrt{1+\delta_e}, \quad \mathcal{K}_e = 1/\sqrt{1+\delta_e}, \\ \delta_e &= (e^2/4\pi\varepsilon_0\hbar v_{\mathrm{F}})[\ln(2/qr_*) - \gamma], \end{aligned} \tag{11}$$

where $\gamma = 0.57721\ldots$ is the Euler constant, r_* is the effective radius of the wire, and ε_0 is the vacuum permittivity (see details in Appendix C or Chapter 4 of Ref. [3]). We also note that both v_e and $\mathcal{K}_e$ are q-dependent. Integration of the electromagnetic field induced by spin modes leads to negligible corrections of the Luttinger parameters on the order of $\delta_\sigma \approx \mu_0\mu_{\mathrm{B}}^2/r_*^2\hbar v_{\mathrm{F}} \sim 10^{-5}$, where we used $r_* \sim 1$ nm and $v_{\mathrm{F}} \sim 10^4$ m/s. As such, in the spin sector, we use

$$\mathcal{K}_\sigma = 1, \quad v_\sigma = v_{\mathrm{F}}. \tag{12}$$

For the quadratic Hamiltonian in Eq. (10), calculation of $\mathcal{C}^{\mathrm{R}}_{\rho_m\rho_m}(q,\omega)$ is straightforward:

$$\mathrm{SU(2)}: \qquad \mathcal{C}^{\mathrm{R}}_{\rho_m\rho_m}(q,\omega) = \frac{2}{\pi}\frac{\mathcal{K}_m v_m q^2}{(v_m q)^2 - (\omega + i\epsilon)^2}, \tag{13}$$

where ϵ is an infinitesimal positive constant.

Using $\mathcal{C}^{\mathrm{R}}_{\rho_m\rho_m}(q,\omega)$ in Eq. (7), we find that the relaxation time induced by charge and spin modes in a LL given by

$$1/T_{1,m}(\omega,T,R) = \frac{(g_{\mathrm{s}}\mu_{\mathrm{B}})^2}{8\pi}\int_0^\infty \frac{dq}{2\pi}F_m(q,y,z,\omega) \times \mathrm{Im}\left[\frac{\coth(\hbar\omega/2k_{\mathrm{B}}T)\mathcal{K}_m v_m q^2}{(v_m q)^2 - (\omega+i\epsilon)^2}\right]. \tag{14}$$

Equation (14) summarizes the essence of magnetic noise measurements in LLs and the key dependencies as a function of experimentally tunable parameters, namely polarization direction, R, and T (for the purposes of current experimental setups, we take ω as fixed). In particular, the probe samples charge and spin fluctuations at all q wave vectors, but only picks those modes, which resonate with the spin probe frequency ω. This feature is manifested by the δ function in the integrand of Eq. (14) introduced by $\mathrm{Im}\{1/[(v_m q)^2 - (\omega + i\epsilon)^2]\} \approx \delta(vq-\omega)/\omega$. Encoded in Eq. (14) is also the ability to measure independently charge and spin noise, which is possible due to the spin degree of freedom of the probe.

To give a gauge of T_1 values encountered in experiments, we evaluate Eq. (14) in the regime $qR \lesssim 1$, such that Eqs. (5) and (6) can be replaced by their asymptotic values, and $\hbar\omega \lesssim k_{\mathrm{B}}T$ such that $\coth(\hbar\omega/2k_{\mathrm{B}}T) \approx 2k_{\mathrm{B}}T/\hbar\omega$. This results in

$$\begin{aligned} \frac{1}{T_{1,e}} &= \frac{(\mu_0\mu_{\mathrm{B}}e)^2}{(2\pi)^2\hbar^3}\frac{g_{\mathrm{s}}^2 k_{\mathrm{B}}T}{R^2}\mathcal{K}_e, \\ \frac{1}{T_{1,\sigma}} &= \frac{(\mu_0\mu_{\mathrm{B}}^2)^2}{(4\pi)^2\hbar^3}\frac{g_{\mathrm{s}}^2 k_{\mathrm{B}}T}{R^4}\frac{g_\sigma^2}{v_{\mathrm{F}}^2}, \end{aligned} \tag{15}$$

where $\mathcal{K}_e$ is evaluated at $q = \omega/v_e$, see Eq. (11). The first factor of $1/T_{1,m}$ is a combination of universal constants reflecting the coupling of charge modes with the spin probe in $T_{1,e}$, and spin-spin coupling in the case of $T_{1,z}$; the second factor contains experimental parameters, namely, the g factor of the probe g_{s}, the probe-to-sample distance R, and temperature (T); the third factor contains 1D system parameters. The relation $1/T_1 \propto g_{\mathrm{s}}^2 kT/\hbar$ resembles the Korringa law [41] apart from geometrical factors which arise because the spin probe is not in the system's bulk.

For estimates, we use $g_{\mathrm{s}} = g_\sigma = 1$, $v_{\mathrm{F}} \sim 10^4$ m/s, $T \sim 100$ K, and $\mathcal{K}_e \sim 1$. This results in a relaxation time given by $1/T_{1,e}$ [s^{-1}] $\approx 10^3/R$ [nm]^2 and $T_{1,z}$ [s^{-1}] $\approx 5\times 10^4/R$ [nm]^4. We note that the relaxation times on the millisecond to ∼10 second range can be accessed with current experimental setups using NV centers in diamond at temperatures around 100 K [42]. We also note that, for typical probe-to-sample distances on the order of a few nanometers, charge and spin noise are comparable, making the spin degree of freedom of the probe essential to separate each contribution. Different noise components can be distinguished, for instance, by measuring relaxation time of differently oriented NV center probes in diamond [17].

1. Relaxation time as a function of distance

For generic R values, the behavior of magnetic noise as a function of distance is straight-forward to obtain because only a single mode with wave vector $q = \omega/v_m$ is being sampled. For $R \lesssim v_m/\omega$, the form factor in the integral of Eq. (14) behaves as $[q^2F_e(q,0,R,\omega)] \approx 1/R^2$, such that the R dependence can be factored out of the integral in Eq. (14), giving rise to a $1/R^2$ power law of $1/T_{1,e}$. Similar analysis is valid for spin noise which gives rise to a $1/R^4$ dependence. At intermediate to large distances, $R \gtrsim v_m/\omega$, noise in Eq. (14) is obtained by integrating the product of the form factor $[q^2F_m(q,0,R,\omega)] \approx qe^{-2qR}/R$, valid for $qR \gtrsim 1$, and the spectral density which is a δ-function at $q = \omega/v_m$. This yields charge and spin relaxation time that falls off exponentially with a characteristic length v_m/ω, $1/T_{1,m}(R) \propto \exp(-2R\omega/v_m)/R$.

2. Relaxation time as a function of temperature

For clean systems, the temperature dependence of noise is governed by the $\coth(\hbar\omega/2k_{\mathrm{B}}T)$ factor in Eq. (14). In particular, for LLs, the spin probe samples ballistic charge

and spin density waves with wave vector $q = \omega/v$. Within the bosonization description, such waves are noninteracting phononlike modes with T-dependent amplitude $|\rho_{e,\sigma}| \propto \sqrt{T}$; this results in charge and spin-induced magnetic noise scaling as $1/T_{1,m}(T) \propto T$ in the semiclassical limit. The linear behavior with T is valid up to $k_B T \approx \hbar\omega$, where noise reaches a minimum value which is due to quantum fluctuations. The latter regime can be captured with NV centers, given that ω is on the range GHz-THz and can be comparable to $k_B T$, and differs from NMR, which operates in the regime $\hbar\omega \ll k_B T$. Both saturation and linear T dependence is captured by the $\coth(\hbar\omega/2k_B T)$ term in Eq. (14). This simple temperature behavior is altered by disorder which introduces nonuniversal power laws, as will be described below.

B. Case II: helical and spin-polarized channels

Spin-polarized states can occur in quantum wires in very strong magnetic fields ($\mu_B B \sim E_F$, with E_F the Fermi energy) or in the presence of ferromagnetic interactions with broken SU(2) symmetry—either due to easy axis or a magnetic field [27,28]. Helical states arise at the edges of 2D systems with strong spin-orbit coupling. Both spin-polarized and helical states introduce several qualitatively distinct behaviors, some of which are discussed in the present section and others in the context of disorder. The 1D motion of spin-polarized or helical fermions can be described with half as many degrees of freedom than in the SU(2) case. In either case, the 1D bosonic action is of the form

$$\mathcal{S}_{1D} = \iint dt dx [\, i\Pi\partial_t\phi - \mathcal{H}_0(\phi, \Pi)]. \tag{16}$$

The bosonized degrees of freedom, Π and ϕ are canonically conjugate, $[\phi(x), \Pi(x')] = i\delta(x - x')$ and describe charge/spin excitations of the 1D system. In the absence of disorder scattering, dynamics is governed by

$$\mathcal{H}_0(\phi, \Pi) = \frac{\hbar v_F}{2\pi}[(\pi\Pi)^2 + (\partial_x\phi)^2]. \tag{17}$$

Similar to the SU(2) case, here we do not include Coulomb repulsion because this is already accounted for in the full action, Eq. (1). In the long-wavelength limit, charge density is related to the bosonized degrees of freedom via $\rho_e = -\partial_x\phi/\pi$. For the spin density ρ_σ, we assume for concreteness that the preferential direction is the z axis (see Fig. 1) such that $\rho_\sigma = \rho_z$. For spin-polarized states, charge and spin densities are equal, $\rho_e = \rho_\sigma = -\partial_x\phi/\pi$; for helical states, spin density is given by $\rho_\sigma = \Pi$. The reason behind this difference is more evident when carrier density is decomposed into its constituent flavors, namely fields $\phi_{r\sigma}$ corresponding to carriers with chirality $r = \pm$, spin polarization $\sigma = \uparrow, \downarrow$, and carrier density $\rho_{r\sigma} = r\partial_x\phi_{r\sigma}/\pi$. Within bosonization, it is standard to define $\phi = -(\phi_{+\sigma} - \phi_{-\sigma'})$ and $\Pi = \partial_x(\phi_{+\sigma} + \phi_{-\sigma'})/2\pi$. As such, for spin-polarized states, the total spin density is obtained by the sum in density of right and left movers, $\rho_\sigma = -\partial_x(\phi_{+\uparrow} + \phi_{-\uparrow})/\pi = \rho_e$. For helical states, on the other hand, the total spin density is obtained by the difference in density of right and left movers, $\rho_\sigma = \partial_x(\phi_{+\uparrow} - \phi_{-\downarrow})/2\pi = \Pi$. Excitations in ρ_x and ρ_y are assumed to be gapped and do not contribute to noise—this is valid so long as T is small compared to the energy scale of the polarizing mechanisms, e.g., ferromagnetism, spin-orbit coupling or Zeeman splitting.

Integration of electromagnetic modes and calculation of charge and spin density correlations proceeds exactly as in the SU(2) case. For spin-polarized states, we find

$$\text{SP}: \quad \mathcal{C}^R_{\rho_m\rho_m}(q,\omega) = \frac{1}{\pi}\frac{\mathcal{K}_e v_e q^2}{(v_e q)^2 - (\omega + i\epsilon)^2}, \quad m = e, \sigma, \tag{18}$$

whereas for helical states, we find

$$\text{helical}: \quad \mathcal{C}^R_{\rho_e\rho_e}(q,\omega) = \frac{1}{\pi}\frac{\mathcal{K}_e v_e q^2}{(v_e q)^2 - (\omega + i\epsilon)^2}$$

$$\mathcal{C}^R_{\rho_\sigma\rho_\sigma}(q,\omega) = \frac{1}{\pi}\frac{v_e q^2/\mathcal{K}_e}{(v_e q)^2 - (\omega + i\epsilon)^2}. \tag{19}$$

In particular, charge correlations have the same form for the spin-polarized, helical, and SU(2) states (albeit a factor of two due to spin degeneracy), see Eq. (15). Spin correlations, however, are different for each of these states:

$$\text{SP}: \quad \frac{1}{T_{1,\sigma}} = \frac{(\mu_0\mu_B^2)^2}{8\pi^2\hbar^3}\frac{g_s^2 k_B T}{R^4}\frac{g_\sigma^2\mathcal{K}_e}{v_e^2},$$

$$\text{helical}: \quad \frac{1}{T_{1,\sigma}} = \frac{(\mu_0\mu_B^2)^2}{8\pi^2\hbar^3}\frac{g_s^2 k_B T}{R^4}\frac{g_\sigma^2}{\mathcal{K}_e v_e^2}. \tag{20}$$

For spin polarized states, because $\rho_\sigma = -\partial_x\phi/\pi$, we find that the amplitude of spin fluctuations is proportional to $\mathcal{K}_e$. For helical states, because $\rho_\sigma = \Pi$, we find that the amplitude of spin fluctuations is proportional to $1/\mathcal{K}_e$. Analysis of the R and T dependence of noise from Eqs. (18) and (19) leads to the same conclusions as in the SU(2) case. The key distinction between SU(2), spin polarized, and helical states in the LL regime is how Coulomb repulsion affect spin noise, as discussed next.

1. Relaxation time as a function of repulsion strength

The internal structure of carriers has interesting manifestations in the spin noise behavior. We illustrate this effect by assuming *in situ* control of $\mathcal{K}_e$ while measuring spin fluctuations. Control of the LL parameters $\mathcal{K}_e$ and v_e can be achieved by using gate potentials, see discussion below. We recall from Eqs. (13), (18), and (19) that the Luttinger parameter $\mathcal{K}_e$ affects the amplitude of spin fluctuations in different ways: spin fluctuations are proportional to $\mathcal{K}_e$ for spin-polarized states, $1/\mathcal{K}_e$ for helical states, and unity for SU(2) states. Physically, this characteristic spin noise behavior can be understood as follows: a spin density for spin-polarized states has to be accompanied by a charge density; as such, both charge and spin density fluctuations are suppressed for stronger Coulomb repulsion [Fig. 2(a)]. A spin density for helical states, on the contrary, can exist in the absence of a charge density; because spin and charge are conjugate fields, Coulomb suppression of charge fluctuations enhances spin fluctuations [Fig. 2(b)]. These two contrasting behaviors, furthermore, are distinct from that in a spinful 1D metal where spin noise is unaffected by long-range Coulomb interactions. As a result, although fluctuations of the charged mode generically decrease at increasing values of $\mathcal{K}_e$, spin noise can either increase (helical phase), remain constant (spinful metal) or

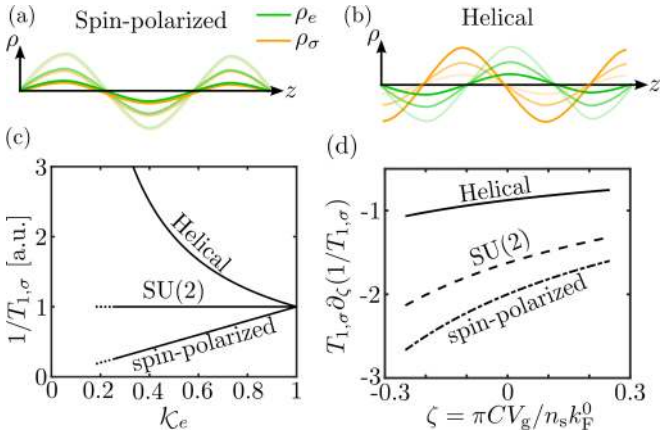

FIG. 2. Effect of tuning repulsion strength on spin noise. (a) Spin fluctuations (orange) for spin-polarized states are locked to charge fluctuations (green); as such, both charge and spin fluctuations are suppressed with increasing Coulomb repulsion (increasing shading of lines). (b) For helical states, it is possible to have finite spin density in the absence of charge density; in this case, spin fluctuations are enhanced with increasing interaction strength. By measuring spin noise while tuning the interaction strength (c) or the gate potential (d) it is possible to distinguish a helical, spin polarized or spinful metal. (Parameters C, n_s, and k_F^0 are defined in the main text.)

decrease (spin polarized phase) depending on the nature of 1D states (Fig. 2).

One possible way to measure the Luttinger liquid parameter and probe the internal structure of 1D carriers is to measure $1/T_{1,\sigma}$ while tuning a gate potential V_g. This modifies both Luttinger parameters $\mathcal{K}_e$ and v_e. The carrier density in a 1D channel can be related to Fermi wave vector k_F and V_g via $n = n_s k_F/\pi = n_s k_F^0/\pi + CV_g$, where k_F^0 is the Fermi wave vector at $V_g = 0$, C is the capacitance between the gate and the 1D system, and n_s is the spin degeneracy of each channel. In terms of the bare Fermi velocity, this relation can be written as $v_F/v_F^0 = 1 + \pi C V_g/n_s k_F^0$. Using Eqs. (15) and (20), combined with the expression for the Luttinger parameters in terms of bare parameters, Eq. (11), the relaxation time can be expressed as $T_{1,\sigma} \propto v_F^2(1+\gamma_2 v_F^0/v_F)^{\gamma_1}$, where $\gamma_1 = 0$ for the SU(2) case, $\gamma_1 = 1/2$ for the helical case, and $\gamma_1 = 3/2$ for the spin-polarized case, and $\gamma_2 = (1-\mathcal{K}_e^0)/\mathcal{K}_e^0$ ($\mathcal{K}_e^0$ is the Luttinger parameter at $V_g = 0$). The power γ_1 and the number γ_2 can be considered as fitting parameters which can be extracted from taking the derivative of $T_{1,\sigma}$ measurements as a function of V_g: $T_{1,\sigma}\partial_\zeta(1/T_{1,\sigma}) = \frac{\gamma_1-2}{1+\zeta} - \frac{\gamma_1}{1+\gamma_2+\zeta}$, with $\zeta = \pi C V_g/n_s k_F^0$, as shown in Fig. 2(d).

IV. NOISE FROM DIRTY WIRES: WEAK DISORDER

Scattering with a disorder potential couples right to left movers. There are two qualitatively distinct types of scattering behaviors, which are usually encountered in 1D systems. The first case, which is discussed in the present section, is when impurities are dense and weak enough such that the effect of a single impurity is negligible but their collective effects are important (Gaussian disorder) [43–45]. The second case, discussed in the next section, is when impurities are scarce but strong (Poisson disorder). Regardless of the details of the scattering potential, it is known that disorder, no matter how weak, gives rise to strong deviations from LL behavior, e.g., Anderson insulators.

Focusing on Gaussian disorder, it is known that charge density waves become pinned by the disorder potential below a characteristic pinning frequency ω_* [44–46]. The value of ω_* is related to the localization length ℓ_{loc} of electron wave functions via $\omega_* = v_e/\ell_{loc}$. Within the long wavelength bosonization description, we can effectively incorporate the effects of disorder to describe quenching of long wavelength fluctuations due to pinning. This approach fails to describe physics occurring at length scales smaller than ℓ_{loc}, as will be described in more detail below. We begin by discussing noise in wires with an SU(2) degree of freedom and Gaussian disorder for $\omega \gtrsim \omega_*$, and compare the resulting noise behavior with that obtained for LLs in the previous section. Afterwards, we discuss qualitatively distinct behaviors that appear in 1D spin-polarized and helical states, also in the regime $\omega \gtrsim \omega_*$. In the final part of this section, we discuss qualitatively distinct behaviors that may arise in the pinned phase, $\omega \lesssim \omega_*$.

A. Case I: SU(2) channels with $\omega \gtrsim \omega_*$

The starting point to discuss disordered wires is the LL Hamiltonian $\mathcal{H}_m$ [Eq. (8)] describing ballistic propagation of charge and spin density waves. We introduce scattering via the disorder potential in bosonized form [47]

$$\mathcal{H}_{dis}(\phi_e, \phi_\sigma) = \frac{u(x)}{\pi a} e^{i\sqrt{2}\phi_e(x)} \cos[\sqrt{2}\phi_\sigma(x)] + \text{H.c.}, \quad (21)$$

which describes spin-conserving backscattering. Here a is the lattice cutoff and $u(x)$ is the continuum limit corresponding to the $2k_F$ components of the scattering potential [3,47]. The potential is assumed to be uncorrelated in space, $\langle u(x)u^*(x')\rangle = D\delta(x-x')$. Importantly, although the potential couples to ρ_e, the long wave-vector backscattering components of the scattering potential also introduces scattering in the spin sector.

The term $\mathcal{H}_{dis}$ introduces competition between two opposite behaviors, namely ballistic propagation of density waves promoted by $\mathcal{H}_0$, and real-space pinning of the charge density promoted by $\mathcal{H}_{dis}$. Pinning of charge density occurs because it is energetically favorable for ϕ_e to track the phase $\phi_{imp}(x)$ of the impurity potential, $u(x) = |u(x)|e^{i\phi_{imp}(x)}$. Several approaches are available to describe scattering in an effective fashion both above and below ω_*, each with its own limitations. To keep the formalism as generic as possible, here we use the memory function formalism, which has been commonly used to obtain correlations in a variety of non-Fermi liquids [46–50].

1. Equations of motion

To describe the effects of disorder, we derive the equations of motion within the memory function formalism, in order to give an intuitive picture of how microscopic dynamics is affected by disorder scattering. The key idea of this approach is to track only a subspace of relevant degrees of freedom, namely, $[\phi_m(q,t), \Pi_m(q,t)]$ for a fixed value of q. The remaining degrees of freedom, which are orthogonal to the subspace spanned by $[\phi_m(q,t), \Pi_m(q,t)]$, enter the equations of motion via fluctuation and dissipation terms. It is clear

from the Hamiltonian $\mathcal{H} = \mathcal{H}_0 + \mathcal{H}_{\rm dis}$, that only $\mathcal{H}_{\rm dis}$ couples $[\phi_m(q,t), \Pi_m(q,t)]$ to their orthogonal subspace. In particular, the operator $f_m = [\mathcal{H}_{\rm dis}, \Pi_m]$ quantifies the leakage out of the subspace spanned by $[\phi_m(q,t), \Pi_m(q,t)]$. Within this approach, the equations of motion $i\partial_t \Pi_m = \frac{1}{\hbar}[\Pi_m, \mathcal{H}]$ and $i\partial_t \phi_m = \frac{1}{\hbar}[\phi_m, \mathcal{H}]$ can be exactly expressed as

$$\partial_t \phi_m(q,t) = \pi \mathcal{K}_m v_m \Pi_m(q,t), \tag{22}$$

$$\partial_t \Pi_m(q,t) = -(v_m q^2/\pi\mathcal{K}_m)\phi_m(q,t) + i\int_0^\infty ds \mathcal{M}_m(q,s)\Pi_m(q,t-s) + \xi_m(q,t). \tag{23}$$

For each value of $m = e, \sigma$, the equations of motion resemble those of a damped harmonic oscillator in which ϕ_m plays the role of position, Π_m of momentum, and $1/\pi\mathcal{K}_m v_m$ of mass. Here, $\mathcal{M}_m(q,t) = \mathcal{M}'_m(q,t) + i\mathcal{M}''_m(q,t)$ is a memory function which introduces dissipation and retardation effects, and $\xi_m(q,t)$ is a random fluctuating force. We note that there is neither memory function nor force term in Eq. (22) because the scattering potential depends on ϕ_m, i.e., $[\mathcal{H}_{\rm dis}(\phi_m), \phi_m] = 0$, but not on Π_m. We also note that coupling between Π_e and Π_σ in Eq. (23) is not present because $\langle f_e f_\sigma \rangle = 0$.

Although Eqs. (22) and (23) are exact [51], calculating the exact form of $\mathcal{M}_m$ and ξ_m is challenging. For this reason, perturbation schemes have been developed to quantify such terms [46]. To leading order in f_m, $\mathcal{M}_m(q,\omega)$ is given by

$$\mathcal{M}_m(q,\omega) = \frac{\mathcal{C}^{\rm R}_{f_m f_m}(q,\omega) - \mathcal{C}^{\rm R}_{f_m f_m}(q,0)}{\omega}. \tag{24}$$

In thermal equilibrium, the fluctuating force and the memory function are not independent. In particular, fluctuations are related to dissipation via the fluctuation-dissipation theorem: $\int_{-\infty}^{\infty} dt e^{i\omega t}\langle \xi_m(-q,t)\xi_m(q,0)\rangle = 2k_{\rm B}T\mathcal{M}''_m(q,\omega)/\pi\hbar v_m \mathcal{K}_m$.

Interpretation of Eqs. (22) and (23) is straightforward when they are rewritten in terms of charge and currents in order to obtain hydrodynamic equations. In particular, by multipying Eq. (22) by $\sqrt{2}q/\pi$, using $\rho_m = -\sqrt{2}\partial\phi_m/\pi$ and $j_m = \sqrt{2}v_{\rm F}\Pi_m = \sqrt{2}\mathcal{K}_m v_m \Pi_m$, we recover the continuity equation, $\partial_t \rho_m = v_m \partial_x j_m$ for charge and spin modes. Similarly, by multiplying Eq. (23) by v_m and assuming for illustrative purposes that the memory function is local in time and purely imaginary, i.e., $i\int_0^\infty ds \mathcal{M}_m(q,s)\Pi_m(q,t-s) = -\nu j_m(q,t)$, we obtain an equation describing current dynamics in a resistive circuit: $\partial_t j_m = v_m^2 \partial_x \rho_m - \nu j_m(x,t) + \xi_m(t)$: the first term in the right-hand side is the driving force for the current (note that $\hbar v_e \partial_x \rho_m = \partial_x \mu$ is the gradient of the chemical potential), the second term is a resistive/dissipative term, and the third term is a random, fluctuating force.

From the equations of motion (22) and (23), it is possible to compute $\mathcal{C}^{\rm R}_{\phi_m\phi_m}(q,\omega)$, from which it is then trivial to obtain $\mathcal{C}^{\rm R}_{\rho_m\rho_m}(q,\omega)$. The first step in this direction is to go into Fourier space and invert Eqs. (22) and (23):

$$\begin{pmatrix}\phi_m \\ \Pi_m\end{pmatrix} = \frac{\xi_m(q,\omega)}{(v_m q)^2 - \omega^2 - \omega\mathcal{M}_m(q,\omega)}\begin{pmatrix}\pi\mathcal{K}_m v_m \\ -i\omega\end{pmatrix}. \tag{25}$$

Obtaining $\mathcal{C}^{\rm R}_{\phi_m\phi_m}(q,\omega)$ via Eq. (25) proceeds in two steps. First, we express the product $\langle \phi_m(q,\omega)\bar{\phi}_m(q,\omega)\rangle$ in terms of $\langle \xi_m(q,\omega)\bar{\xi}_m(q,\omega)\rangle$, which can be obtained from the fluctuation-dissipation theorem: $\langle \xi_m(q,\omega)\bar{\xi}_m(q,\omega)\rangle = 2k_{\rm B}T\mathcal{M}''_m(q,\omega)/\pi\hbar v_m\mathcal{K}_m$. Second, we make the connection between correlation functions $\langle \phi_m(q,\omega)\bar{\phi}_m(q,\omega)\rangle = \frac{2k_{\rm B}T}{\hbar\omega}{\rm Im}[\mathcal{C}^{\rm R}_{\phi_m\phi_m}(q,\omega)]$, which is valid in thermal equilibrium and in the classical limit $k_{\rm B}T \gg \hbar\omega$. These two steps result in

$$\mathcal{C}^{\rm R}_{\phi_m\phi_m}(q,\omega) = \frac{\pi\mathcal{K}_m v_m}{(v_m q)^2 - \omega^2 - \omega\mathcal{M}_m(q,\omega)}. \tag{26}$$

From here, it is trivial to obtain charge and spin density correlators by using the mapping $\rho_m = \sqrt{2}\partial_x\phi_m/\pi$, which results in

$${\rm SU(2)}: \mathcal{C}^{\rm R}_{\rho_m\rho_m}(q,\omega) = \frac{2}{\pi}\frac{\mathcal{K}_m v_m q^2}{(v_m q)^2 - \omega^2 - \omega\mathcal{M}_m(q,\omega)}. \tag{27}$$

2. Memory functions for disorder scattering

Because the disorder potential is short-ranged and Gaussian, $\mathcal{M}_m(q,\omega)$ does not depend explicitly on q (see Appendix D); $\mathcal{M}(q,\omega)$ does have, however, an implicit q-dependence via $\mathcal{K}_e$ and v_e [cf. Eq. (11)]. Further, because $\mathcal{M}_m(q,\omega)$ depends on the temperature of the system, hereafter we show these dependencies explicitly, $\mathcal{M}_m(q,\omega) \equiv \mathcal{M}_m(q,\omega,T)$.

The memory function can be generically written as

$$\mathcal{M}_m(q,\omega,T) = \Gamma_m\left(\frac{ak_{\rm B}T}{\hbar v_m}\right)^{\alpha_m}\mathcal{F}_m\left(\frac{\hbar\omega}{k_{\rm B}T}\right),\ m = e,\sigma, \tag{28}$$

where Γ_m is a constant with units of $\sec^{-1}$, α_m is a number that depends on microscopics, and $\mathcal{F}_m(x)$ is a dimensionless complex function. The details of the memory functions calculation are given in Appendix D. Given that spin probes usually operate with ω below THz frequencies ($\lesssim$4 meV) and temperatures can vary over a wide range including room temperatures, we focus on the regime $\hbar\omega \lesssim k_{\rm B}T$, which is mostly relevant to experiments. In this regime, we find that $\mathcal{F}_m(x \lesssim 1)$ is approximately constant and, therefore, the sign of α_m determines whether the scattering rate increases or decreases with temperature. In particular, the memory function behaves as $\mathcal{M}_m(q,\omega,T) \approx i\beta\Gamma_m(ak_{\rm B}T/\hbar v_m)^{\mathcal{K}_e+\mathcal{K}_\sigma-2}$, where $\Gamma_e = (2\pi)^{\mathcal{K}_e+\mathcal{K}_\sigma+1}D\mathcal{K}_e^2(v_e/v_\sigma)^{\mathcal{K}_\sigma}$ and $\Gamma_\sigma = (2\pi)^{\mathcal{K}_e+\mathcal{K}_\sigma+1}D\mathcal{K}_\sigma^2(v_\sigma/v_e)^{\mathcal{K}_e}$ (the values of $\mathcal{K}_e$ and v_e are q-dependent). Because for repulsive interactions $\mathcal{K}_e + \mathcal{K}_\sigma - 2 < 0$ is valid, $\mathcal{M}_m(q,T)$ (and the scattering rate) monotonically decreases as a function of T. As such, the system behaves more "ballistic"-like as temperature increases.

3. Magnetic noise from disordered wires

Combining Eqs. (27) and (7), we find a relaxation time induced by charge and spin modes given by

$$1/T_{1,m}(\omega,T,R) = \frac{(g_{\rm s}\mu_{\rm B})^2}{8\pi}\int_0^\infty \frac{dq}{2\pi}F_m(q,0,R,\omega) \times \frac{\coth(\hbar\omega/2k_{\rm B}T)\mathcal{K}_m v_m q^2 \omega\mathcal{M}''_m(q,\omega,T)}{[(v_m q)^2 - \omega^2 - \omega\mathcal{M}'(q,\omega,T)]^2 + [\omega\mathcal{M}''_m(q,\omega,T)]^2}. \tag{29}$$

Equation (29) summarizes the essence of magnetic noise measurements in the presence of disorder. In particular, disorder couples modes with different q wave vectors and, as such, charge and spin fluctuations at frequency ω are distributed in q space. This is qualitatively distinct from clean systems where fluctuations with frequency ω are dominated by a single wave vector ω/v_m.

In order to simplify the discussion, in what follows we fix the values of $\mathcal{K}_e$ and v_e appearing in $\mathcal{M}_m$ such that $\mathcal{M}_m$ no longer depends implicitly on q. This approximation is valid when scattering rate is small, $\omega \gtrsim \mathcal{M}''_m$, given that most of the contribution to noise in Eq. (29) comes from a small phase space region centered at $q = \omega/v_e$ for $1/T_{1,e}$, and $q = \omega/v_F$ for $1/T_{1,\sigma}$. For large scattering rate, $\omega \lesssim \mathcal{M}''$, a larger region in q space contributes to noise and, as such, there will be q-dependent logarithmic corrections to $\mathcal{K}_e$ and v_e. We neglect these secondary corrections, which do not alter the qualitative behavior, but that could easily be incorporated if a detailed quantitative analysis were needed. The distribution of modes in q space modifies the dependence of magnetic noise as a function of distance found for LLs and, furthermore, results in nonuniversal power law of T, as will be discussed next.

4. Relaxation time as a function of distance

We begin the analysis of Eq. (29) by exploring how modes in disordered wires are sampled as the probe-to-sample distance is changed. Let us focus on charge-induced noise, and focus on the regime $k_BT/\hbar \gtrsim \omega \gtrsim \omega_*$, where it is valid to assume that $\mathcal{M}''_m(\omega, T) \gg \mathcal{M}'_m(\omega, T)$ [see paragraph following Eq. (28)]. We also assume that scattering rate is large, $\omega \lesssim \mathcal{M}''_m(\omega, T)$, such that density waves start to become pinned by disorder and depart from the LL behavior discussed in the previous section. Figure 3(a) shows charge-induced noise as a function of distance from the disordered wire, and the results are compared to those for clean wires. We recall that, for LLs, noise decays as $1/R^2$ until R becomes comparable to the excitations wavelength ω/v_e; beyond this length, magnetic noise decays exponentially as a function of distance. For disordered wires at close proximity we find that magnetic noise also decays as $1/R^2$ so long as $R \lesssim \ell_d = v_m/\sqrt{\omega\mathcal{M}_m}$, where ℓ_d is the scattering length, but its overall magnitude is smaller due to charge pinning. Interestingly, we find that for $R \gtrsim \ell_d$, magnetic noise in a disordered wire decays as a $1/R^3$ power law and can overwhelm magnetic noise for clean wires, which decays exponentially with R.

This behavior can be understood as follows. In the regime in which backscattering dominates, the denominator of the integrand in Eq. (29) is dominated by the scattering rate $\omega\mathcal{M}''_m$, and can be approximated as $\sim 1/[(v_mq)^4 + (\omega\mathcal{M}''_m)^2]$. As such, the relaxation time integral in Eq. (29) can be written as $\int_0^\infty dq\, F_e(q, 0, R, \omega)\mathcal{M}''_m/[(v_mq)^4 + (\omega\mathcal{M}''_m)^2]$. For $R \lesssim \ell_d$, we can use $F_e(q, 0, R, \omega) \sim 1/(qR)^2$, from which a $1/R^2$ dependence is obtained by pulling the $1/R^2$ factor out of the integral. For $R \gtrsim \ell_d$, we can make the integral dimensionless by defining $x = qR$ and using $\omega\mathcal{M}''_e/R^2 \ll 1$ in the denominator, which results in a $1/R^3$ power-law behavior, $1/T_{1,e} = [e^2\mathcal{K}\omega^2\ell_d^2/8\pi^2v^2R^3]\int_0^\infty dx x^2K_1^2(x)$ [see Fig. 3(b)]. As such, the exponential versus power-law behavior of noise as a function of probe-to-sample distance can be used as diagnostics of pinning of density waves.

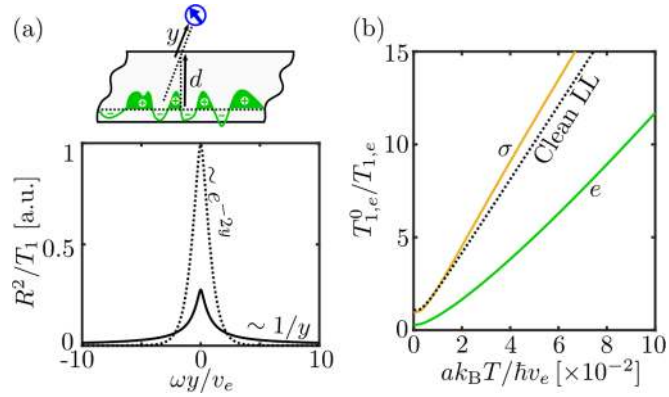

FIG. 3. (a) Qualitatively distinct noise behaviors as a function of probe-to-sample distance for clean (dotted line) and disordered (solid line) systems. Clean systems exhibit an exponentially decay of noise as a function of R governed by the length scale v_e/ω. For disordered systems, we find noise decaying as y^{-3} power law (see discussion in main text). Here we assume that the spin probe is positioned at $\boldsymbol{r} = (0, y, d)$ and the 1D system runs in the $\boldsymbol{r} = (x, 0, 0)$ line. (b) The temperature dependence of the relaxation time exhibits nonuniversal power-law behavior. Temperature combined with interactions makes the system less susceptible to scattering and, as a result, enhances magnetic noise. For $\hbar\omega \lesssim k_BT$, we find superlinear (sublinear) T dependence of charge(spin) noise. Here, $T^0_{1,e}$ relaxation time due to quantum fluctuations in a clean wire.

5. Relaxation time as a function of temperature: emergence of non-universal power laws

Disorder results in the emergence of nonuniversal power-laws of T, one of the key signature of LL. Again, let us focus on the regime $k_BT/\hbar \gtrsim \omega \gtrsim \omega_*$, where $\mathcal{M}_m(\omega, T)$ is strongly T-dependent and it is valid to assume $\mathcal{M}''_m(\omega, T) \gg \mathcal{M}'_m(\omega, T)$. We also assume that the scattering rate is large, $\mathcal{M}''_m(\omega, T) \gtrsim \omega$, such that we are away from LL behavior. Figure 3(b) shows the dependence of the relaxation time as a function of T, and the results are compared with those of clean LLs, which is governed by a $\coth(\hbar\omega/2k_BT)$ factor. Results are plotted assuming that the probe is close to the sample, $R/\ell_{dis} \lesssim 1$. We find that $1/T_1$ has nonuniversal power law behavior, with charge noise behaving superlinerly, whereas spin noise behaves sublinearly. This behavior can be understood as follows. In the regime in which backscattering dominates, the denominator in Eq. (29) can be approximated using $1/[(v_mq)^4 + (\omega\mathcal{M}''_m)^2]$ and the integral in q space can be expressed as $1/T_{1,m} \propto \int_0^\infty dqq^r/[(v_mq)^4 + (\omega\mathcal{M}''_m)^2]$, where $r = 0$ for $m = e$ and $r = 2$ for $m = \sigma$. The relaxation time integral can be made dimensionless by defining $x = v_mq/\sqrt{\omega\mathcal{M}''_m}$ such that all T-dependent terms appear as prefactors of the integral. Upon normalization, Eq. (29) gives rise to noise scaling with temperature as $1/T_{1,e}(T) \propto T/\sqrt{\mathcal{M}''_m(T)}$, and spin noise scaling as $1/T_{1,\sigma}(T) \propto T\sqrt{\mathcal{M}''_m(T)}$, where the factor T is introduced by the $\coth(\hbar\omega/2k_BT) \approx 2k_BT/\hbar\omega$ term in the numerator of Eq. (29). Using $\mathcal{M}_m(\omega, T)$ in Eq. (28) for $k_BT \gtrsim \hbar\omega$,

we find that, when scattering rate is large, charge-induced noise increases superlinearly with T, $1/T_{1,e} \propto T^{2-(\mathcal{K}_e+\mathcal{K}_\sigma)/2}$, whereas spin noise increases sublinearly with T, $1/T_{1,\sigma} \propto T^{(\mathcal{K}_e+\mathcal{K}_\sigma)/2}$. We also note that charge fluctuations depend on $\mathcal{K}_\sigma$ (and viceversa) because the scattering potential in Eq. (21) couples the charge and spin degrees of freedom.

B. Case II: helical and spin-polarized channels with $\omega \gtrsim \omega_*$

The starting point to discuss disordered spin-polarized and helical states is the LL Hamiltonian, Eq. (17), describing ballistic propagation of charge/spin density waves. Proceeding with our minimal approach, we introduce scattering via a disorder potential of the form [43]

$$\mathcal{H}_{\rm dis}(\phi) = \frac{u_n(x)}{\pi a} e^{2in\phi(x)} + \text{H.c.} \tag{30}$$

Here, a is the lattice cutoff and $u_n(x)$ is an uncorrelated potential $\langle u_n(x)\bar{u}_n(x')\rangle = D_n\delta(x-x')$. The value of $n = 1, 2$ reflects the amount of particles involved in scattering and captures two qualitatively distinct noise behaviors. The case $n = 1$ corresponds to the usual direct backscattering term where $u_1(x)$ is the continuum limit of the $2k_{\rm F}$ components of the scattering potential [3]. It is often the case, however, that symmetries of the Hamiltonian do not allow such terms, e.g., in the quantum spin Hall states wherein helical states are protected from backscattering by time-reversal symmetry. Rather than specifying one of the several microscopic models which have been proposed [30,33,34], here instead we capture scattering phenomenologically by using $n = 2$ in Eq. (8), resembling two particles participating in the backscattering process, and $u_2(x)$ is an effective potential induced by second order processes. As we will see, the key effect of n is to describe whether temperature combined with interactions enhances or quenches backscattering.

The equations of motion for the helical and spin-polarized states are the same as those for the SU(2), Eqs. (22) and (23) but, because the spin degree of freedom is frozen, restricted to the charge sector $m = e$. As such, we do not repeat the same procedure that lead to Eqs. (22)–(27), but only quote the final result. For spin-polarized states, we find

$$\text{SP}: \quad \mathcal{C}^{\rm R}_{\rho_m\rho_m}(q,\omega,T) = \frac{1}{\pi}\frac{\mathcal{K}_e v_e q^2}{(v_e q)^2 - \omega^2 - \omega\mathcal{M}_1(\omega,T)}, \tag{31}$$

where we used the relation $\rho_e = \rho_\sigma$, and $\mathcal{M}_1$ is the memory function corresponding to the scattering potential in Eq. (30) for $n = 1$. For helical states, we have to keep in mind that the correlator $\mathcal{C}^{\rm R}_{\rho_\sigma\rho_\sigma}(q,\omega)$ is obtained from $\mathcal{C}^{\rm R}_{\Pi\Pi}(q,\omega)$, see Eq. (25), which results in

$$\begin{aligned}\text{helical}: \ \mathcal{C}^{\rm R}_{\rho_e\rho_e}(q,\omega,T) &= \frac{1}{\pi}\frac{\mathcal{K}_e v_e q^2}{(v_e q)^2 - \omega^2 - \omega\mathcal{M}_2(\omega,T)},\\ \mathcal{C}^{\rm R}_{\rho_\sigma\rho_\sigma}(q,\omega,T) &= \frac{1}{\pi}\frac{\omega^2/\mathcal{K}_e v_e}{(v_e q)^2 - \omega^2 - \omega\mathcal{M}_2(\omega,T)}.\end{aligned} \tag{32}$$

Here, $\mathcal{M}_2(q,\omega)$ is the memory function corresponding to Eq. (30) for $n = 2$.

To give a qualitative picture of the temperature dependence of $\mathcal{M}_n(\omega,T)$, we quote the results in the regime $\hbar\omega \lesssim k_{\rm B}T$ (details for all values of ω, T are described in the Appendix D). In this regime, we find $\mathcal{M}_n(\omega,T) \approx i\gamma_n(ak_{\rm B}T/\hbar v_e)^{2n\mathcal{K}_e-2}$, where $\gamma_n = (2\pi)^{2n\mathcal{K}_e-2}(D_n\mathcal{K}_e/v_e)$. For $n = 1$, any value of repulsive interaction makes the scattering rate monotonically decreasing as a function of T; this behavior is the same as in the SU(2) case. This indicates that interactions combined with temperature tend to make the system less sensitive to the disorder. For $n = 2$, there is a transition in the temperature dependence of the $\mathcal{M}_2(\omega,T)$, which occurs at $\mathcal{K}_{\rm c} = 1/2$: scattering is enhanced (suppressed) at larger temperatures for $\mathcal{K}_e > \mathcal{K}_{\rm c}(\mathcal{K}_e < \mathcal{K}_{\rm c})$. The existence of a critical repulsion strength which changes the importance of scattering at small temperatures is consistent with proposed microscopic models of scattering in quantum spin Hall phases (the value of $\mathcal{K}_{\rm c}$, however, is model specific).

The analysis of how noise varies as a function of distance for disordered wires leads to the same power-law behaviors as those in the SU(2) case described in the previous section, so we do not reproduce the results here. Instead, here we focus on how single particle backscattering and interaction-assisted backscattering lead to qualitatively distinct noise behaviors as a function of T.

1. *Relaxation time as a function of temperature*

We consider first the case of single particle backscattering, $n = 1$ in Eq. (21), wherein temperature makes modes less sensitive to disorder. As before, we focus on the regime $k_{\rm B}T/\hbar \gtrsim \omega \gtrsim \omega_*$, where $\mathcal{M}_1(\omega,T)$ is strongly T-dependent and it is legitimate to assume $\mathcal{M}_1''(\omega,T) \gg \mathcal{M}_1'(\omega,T)$ [see paragraph following Eq. (28)], and also that scattering rate is large, $\omega \lesssim \mathcal{M}_1''(q,\omega)$, such that we deviate from LL behavior discussed in the previous section. Figure 4(a) shows the dependence of the relaxation time as a function of T for the spin-polarized case, and the results are compared with those of clean LLs. The T dependence of noise follows the same behavior as in the disordered wire with an SU(2) degree of freedom, see Fig. 3(b), but with a power law that depends only on $\mathcal{K}_e$. In particular, upon normalization and pulling out all the T-dependent terms of the integral, Eq. (14) gives rise to noise scaling with temperature as $1/T_{1,e}(T) \propto T/\sqrt{\mathcal{M}_1''(T)}$, and spin noise scaling as $1/T_{1,\sigma}(T) \propto T\sqrt{\mathcal{M}_1''(T)}$. Using $\mathcal{M}_1(\omega,T)$ described in the previous section for $k_{\rm B}T \gtrsim \hbar\omega$, we find that charge-induced noise increases superlinearly with T, $1/T_{1,e} \propto T^{2-\mathcal{K}_e}$, whereas spin noise increases sublinearly with T, $1/T_{1,\sigma} \propto T^{\mathcal{K}_e}$ [see Fig. 4(a) at moderate to high T].

Helical states exhibit qualitatively distinct noise behavior as a function of T than the spin-polarized case for weak repulsion, $\mathcal{K}_e > 1/2$, see Fig. 4(b). For small T, time-reversal symmetry protects chiral states against backscattering; this leads to a clean LL behavior at $T = 0$. At large T, multiparticle interactions *assist* disorder in backscattering chiral states, resulting in an enhancement of the scattering rate. To roughly estimate the T dependence when scattering rate is strong, we note the magnetic noise integral in q space in Eq. (29) can be approximated as $\int_0^\infty dq\,\mathcal{M}_2''/[(v_m q)^4 + (\omega\mathcal{M}_2'')^2]$, where we used the same approximations as in the previous paragraph.

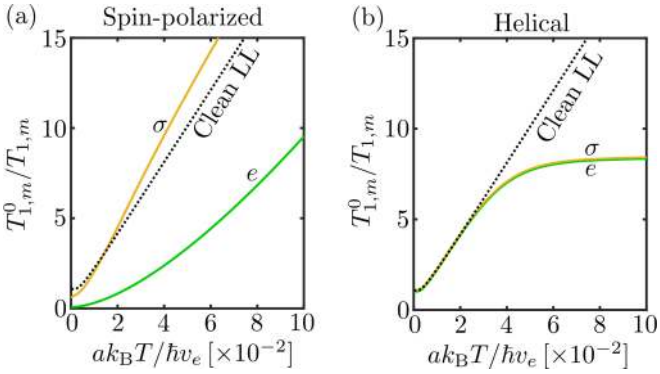

FIG. 4. The temperature dependence of the relaxation time due to charge ($m = e$) and spin ($m = \sigma$) modes exhibits nonuniversal and qualitatively distinct behaviors for different microscopic phases and scattering mechanisms. (a) For the disordered spin-polarized phase at $T = 0$, backscattering leads to localization and suppression of charge and spin density fluctuations. Temperature combined with interactions makes the system less susceptible to scattering and enhances magnetic noise. For $\hbar\omega \lesssim k_BT$, we find superlinear (sublinear) T dependence of charge(spin) noise. (b) In the helical phase, because of time-reversal symmetry, disorder backscattering is suppressed at $T = 0$ and the system behaves as a perfect LL. Temperature combined with interactions assists disorder backscattering. For weak repulsion, we find sublinear (superlinear) T dependence of charge (spin) noise, see details in main text. In the figures, we use $a\omega/v = 5 \times 10^{-3}$.

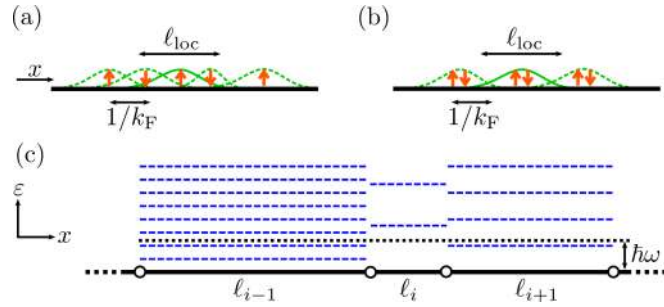

FIG. 5. (a) Pinning of wave functions leads to quenching of charge fluctuations. For strong repulsion, neighboring spins are coupled via an antiferromagnetic coupling and spin fluctuations are possible. (b) For weak repulsion, spin form singlet states and spin fluctuations become gapped. (c) Spatial inhomogeneity and detuning of noise in the strong impurity regime. For strong, sparse impurities (empty circles), the wire is cut into segments of size ℓ_i and finite-size quantization effects, $\Delta\varepsilon_i = \hbar v/\ell_i$, take place. If the level splitting of the probe ω is sufficiently detuned from $\Delta\varepsilon_i$, the relaxation time becomes negligibly small.

The key distinction with the spin-polarized case is that $\mathcal{C}^{\rm R}_{\rho_\sigma\rho_\sigma}$ in Eq. (31) contains an ω^2 term in the numerator rather than a q^2 term, thus the sampling weight in q-space is different than in the spin-polarized case. As such, we find a relaxation time scaling with temperature as $1/T_{1,m}(T) \propto T/\sqrt{\mathcal{M}''_2(T)}$. For $\hbar\omega \lesssim k_BT$, we find a sublinear T-dependent behavior for the relaxation time, $1/T_{1,m}(T) \propto T^{2(1-\mathcal{K}_e)}$.

A subtle yet interesting effect is that, because spin fluctuations are locked to charge fluctuations for spin-polarized and helical states, the magnetic noise due to charge and spin modes as a function of temperature are also locked. Using the scaling as a function of T found above, for spin polarized states, we find that the product $1/T_{1,e}T_{1,\sigma}T^2$ is independent of T, whereas for helical states, the product $T_{1,e}/T_{1,\sigma}$ is independent of T. This behavior suggests a diagnostics of helical versus spin-polarized 1D channels. A similar behavior was discussed above for the SU(2) case for strong disorder, where the charge and spin sectors become coupled by the scattering potential, Eq. (30). For more general 1D systems where charge and spin degree of freedom are separated and subject to different scattering potentials, e.g., Hubbard models, charge and spin noise are no longer locked.

C. Case III: 1D channels with $\omega \lesssim \omega_*$

While memory functions correctly capture qualitatively behaviors which are important for our discussion, such as enhancement/quenching of scattering as a function of temperatures, there are more accurate approaches to describe the dependence on T and ω particularly in the regime $\omega \lesssim \omega_*$. The key limitation of Eq. (24) is that, as soon as ω approaches ω_*, higher order corrections (in powers of f_m) become necessary. One way to tackle this problem is to combine the memory function formalism with RG [47], such that the microscopic parameters $\mathcal{K}_m$, v_m, and D_m, which are constant in our model, become T-dependent. This approach, however, fails to describe physics on the scale of $\ell_{\rm loc}$ which are important if the probe is located within $R \lesssim \ell_{\rm loc}$.

Another approach, which is valid when $k_BT \lesssim \hbar\omega \ll \omega_*$, is the Gaussian variational approach, which consists of finding the best quadratic approximation to the disordered Hamiltonian via minimization in replica-space, in order to compute two-point correlations [45]. Replica-symmetry-breaking generates a mass term in the excitation spectrum, which can be described by replacing $-\omega\mathcal{M} \to M + i\gamma\omega$ in Eq. (31), where M is a mass term and γ is a T-dependent factor. The imaginary term $i\gamma\omega$ gives rise to the characteristic $\sigma(\omega) \propto \omega^2$, which governs conductivity in 1D systems, and qualitatively agrees with the usual $\sigma(\omega) \sim \omega^2\ln^2\omega$ obtained in the Anderson insulating regime ($\mathcal{K}_e = 1$) as well as in the Fukuyama-Lee regime ($\mathcal{K}_e = 0$) [44]. Contrary to RG, this approach fails to account for the renormalization of the Luttinger parameters. Further, it also fails to describe charge motion via quantum creep, which gives rise to variable range hopping [52,53].

Both RG and the Gaussian variational approach are good to describe quenching of long wavelength charge and spin fluctuations. Both approaches, however, rely on self-averaging of the disorder potential. This approximation may become questionable when accessing dynamics at distances $R \lesssim \ell_{\rm loc}$. In particular, while we still expect orbital degrees of freedom to become frozen as the wave function becomes localized in space due to disorder, the spin degree of freedom can still fluctuate; long wavelength spin fluctuations are quenched, but spin fluctuations on the lattice scale remain, e.g., paramagnetic fluctuations. If Coulomb repulsion is sufficiently strong, interactions between neighboring spins are antiferromagnetic, and each spin interacts with $\sim k_F\ell_{\rm loc}$ nearest neighbors via random exchange parameters, see Fig. 5(a). This creates

islands—or rare regions—where spins are strongly correlated (for a general discussion of spin fluctuations in disordered systems, see Ref. [54]). As such, spin probes can detect spin-induced noise induced by paramagentic fluctuations in these islands, so long as the probe-to-sample distance is on the order of island size. For weak repulsion, it has been shown that localization can also lead to localized singlet states in which spin fluctuations become gapped, see Fig. 5(b) [47]. In this case, spin induced noise is quenched even on the scale $\ell_{\rm loc}$.

V. NOISE FROM DIRTY WIRES: STRONG IMPURTIES

A different disorder regime is present when impurities introduce strong, local scattering potentials which are, on average, sufficiently separated from each other. In this regime, a scattering potential of the form $U(x) = \sum_i u_i \delta(x - x_i)$ is assumed, such that the separation of impurities is large on the lattice and excitation wavelength scale, $\ell_i = x_{i+1} - x_i \gtrsim v/\omega \gg a$. Further, we assume that u_i/a is weak compared with Fermi energy of 1D electronic states such that bosonization is still valid, but large compared to ω. Let us focus first on the spin-polarized phase. Within the bosonization description, the impurity Hamiltonian introduced by $U(x)$ can be written as

$$\mathcal{H}_{\rm imp} = \sum_i \frac{u_i}{\pi a} \cos[2\phi(x = x_i)], \tag{33}$$

where unimportant forward-scattering terms are removed. Following Kane and Fisher [55,56], the key effect of Eq. (33) is to pin $\phi(x)$ to the impurity potential at the positions x_i. Because impurities are relevant for $\mathcal{K}_e < 1$, for small enough temperatures, the system flows to strong coupling (in the RG sense) and can be interpreted as a set of finite, decoupled 1D metallic segments; there is zero transmission across the impurity at $T = 0$, and a power law behavior as a function of T.

Under this simplistic picture, we expect two main effects on the relaxation time behavior in the strong disorder regime. First, finite-size quantization effects for each segment will take place such that the energy level splitting of the segments will be, on average, $\Delta\varepsilon \sim \hbar v n_{\rm imp}$, with $n_{\rm imp}$ the impurity density. As such, if $\omega \lesssim \Delta\varepsilon$, then the probe will unlikely couple to the sample. More quantitatively, the probability of finding a segment of size $\ell_i \geqslant v/\omega$ is exponentially small, $p \sim \exp(-n_{\rm imp}\ell_i)$. This analysis allows to define a minimum segment size in order to couple the spin probe to the sample. For instance, for sub-THz frequencies, we expect the minimun segment size to be on the order of $\ell_i \gtrsim v/\omega \sim 100$ nm (here we used $v = 10^4$ m/s and $\omega \lesssim 100$ GHz).

Second, because the distribution of lengths in each segment is expected to be random, we also expect highly inhomogeneous magnetic noise as a function of x. This is qualitatively different than the weak disorder case where, because the probe samples a large number of defects which are available within a distance R, noise is expected to be relatively homogeneous across x due to self-averaging.

Introducing an SU(2) degree of freedom leads to the same conclusions as the spin polarized state, namely, charge and spin density waves are perfectly reflected at the impurity for any value of repulsive interactions (for small enough T). Interestingly, if one breaks the SU(2) spin symmetry but preserves a spin U(1), then mixed phase are possible in which charge density waves are perfectly reflected and spin density waves are perfectly transmitted (or vice versa) [55]. By separating charge and spin fluctuations, this peculiar behavior can potentially be detected with spin probes.

VI. BEYOND THE MINIMAL TWO-CHANNEL MODEL

One-dimensional systems can feature physics beyond our minimal two-channel model. The simplest extension to our model is adding orbital degrees of freedom, for instance, ladders or carbon nanotubes. Extension of our formalism to these cases follow the same lines as in the SU(2) spin degree of freedom case, i.e., increasing the number of fields, all of which satisfy Eq. (8) separately but with orbital-dependent Luttinger parameters. The large range of possibilities available for coupling the degrees of freedom via scattering or interactions give rise to a wide range of regimes in which noise can be dominated by different types of fluctuations, e.g., superconducting or ferromagentic fluctuations.

In addition, although our attention was mainly on the qualitative features of noise, 1D physics is sensitive to microscopic details. It is often the case that several microscopic models explain, up to some degree, some experimental observation. Two notable examples are non-quantized conductivity for quantum spin Hall states, and the case of the 0.7 anomaly observed in conductance measurements in quantum wires [57–59]. In the former case, several backscattering mechanism have been proposed for quantum spin Hall states, such as trapping of electrons in quantum dots, or disordered Rashba coupling [30–35]. In the latter case, two opposite pictures, namely a transition into a 1D Wigner crystal and the formation of a Kondo impurity, have been proposed to explain the data. By exploiting *both* the spatial and spectral (via T) resolution of spin probes, it may be possible to shed light on the operating mechanisms in these two interesting and somewhat controversial cases.

In addition, low-energy excitations may exhibit quasi-1D behavior. Such is the case of edges in the quantum Hall regime and edge magnetoplasmon, wherein charge density fluctuations at the edge induce not only edge currents but also bulk currents [60]. While the above discussion remains valid, it is now necessary to account for lateral currents (towards the bulk) in addition to the already studied edge currents. While not pursued here, an intriguing possibility is using spin probes to map the conducting channels in quantum Hall systems.

VII. SUMMARY

The ability to sample charge and spin fluctuations in a wide range of length scales render spin probes an invaluable probing technique of 1D systems, particularly when the coupling between charge and spin modes is important. We outlined protocols that exploit the spin degree of freedom of the probe to measure charge and spin fluctuations in a wide range of 1D systems. Furthermore, we discussed the effects of scattering, interactions and internal structures of 1D carriers on temperature and probe-to-sample distance dependence of noise. We showed that these features can be accessed using

readily available NV-based diamond probes. In the same spirit, spin probes are also promising candidates to explore a whole zoo of phenomena in 1D systems, such as Kondo impurities and ladders, thus opening intriguing new pathways to access charge and spin fluctuations in general 1D systems.

ACKNOWLEDGMENTS

We thank J. Sanchez-Yamagishi, T. Andersen, C. Bolech, V. Kasper, R. Schmidt, and S. Chatterjee for valuable insights and discussions. J.F.R.-N., and E.D. acknowledge support from the Harvard-MIT CUA, NSF Grant No. DMR-1308435, and AFOSR-MURI: Photonic Quantum Matter, award FA95501610323. K.A. acknowledges support from the DOE-BES Grant No. DE-SC0002140, and the U.K. Foundation. T.G. acknowledges support by the Swiss National Science Foundation under Division II. B.I.H. acknowledges support from the STC Center for Integrated Quantum Materials, NSF grant DMR-1231319. M.D.L. acknowledges support from the Harvard-MIT CUA, the Vannevar Bush Fellowship, and the Moore Foundation.

APPENDIX A: RELAXATION RATE OF THE SPIN PROBE

There are two important protocols used to study magnetometry in solid-state system. In the first approach, static magnetic fields can be measured by determining the Zeeman splitting of the spin probe. This approach, which allows to observe magnetic textures, has been used for single spin imaging [61] and domain walls [62]. In the second approach, which is the one discussed in the present work, the relaxation time of a spin-probe prepared in a pure state is measured.

The relaxation time is governed by the time-dependent Hamiltonian $\mathcal{H}_{\rm spin} = (\hbar\omega/2)\sigma_z + g_s\mu_B\boldsymbol{\sigma}\cdot\boldsymbol{B}(t)$, where we assume a spin-1/2 probe with an intrinsic level splitting $\hbar\omega$. Without loss of generality, we assume that the intrinsic polarizing field is in the $\hat{z}$ direction (here, g_s is the probe g factor, μ_B the Bohr magneton, and $\boldsymbol{B}(t)$ the wire-induced magnetic field). We also assume that the 1D system is in thermal equilibrium, described by the density matrix $\rho_{1D} = \sum_n \rho_n |n\rangle\langle n|$, where n are eigenstates with energy ε_n and $\rho_n = e^{-\varepsilon_n/k_BT}$. The absorption rate $1/T_{\rm abs}$ and emission rate $1/T_{\rm em}$ is obtained from Fermi Golden's rule using the initial state $|i\rangle = |-\rangle\otimes\rho_{1D}$ and $|i\rangle = |+\rangle\otimes\rho_{1D}$:

$$1/T_{\rm abs,em} = \frac{2\pi(g_s\mu_B)^2}{\hbar}\sum_{nm}\rho_n B^{\pm}_{nm}B^{\mp}_{mn}\delta(\omega\mp\varepsilon_{nm}). \quad \text{(A1)}$$

Here, $B^{\pm}_{nm}$ denotes $\langle n|B^{\pm}|m\rangle$, with $B^{\pm} = B^x \pm iB^y$, and ε_{mn} is the energy difference between states n and m, $\varepsilon_{nm} = \varepsilon_n - \varepsilon_m$. The relaxation rate is defined as $2/T_1 = [1/T_{\rm abs} + 1/T_{\rm em}]$. It is straightforward from Eq. (A1) that $1/T_1$ and can be expressed in terms of the anticommutator

$$\frac{1}{T_1} = \frac{(g\mu_B)^2}{2\hbar^2}\int_{-\infty}^{\infty} dt e^{i\omega t}\langle\{B^-(t), B^+(0)\}\rangle. \quad \text{(A2)}$$

For calculation purposes, it is convenient to cast Eq. (A2) in terms of retarded correlation functions. As such, we use the fluctuation-dissipation theorem to express the correlation function in Eq. (A2) as

$$\int_{-\infty}^{\infty} dt e^{i\omega t}\langle\{B^-(t), B^+(0)\}\rangle = \coth\left(\frac{\hbar\omega}{2k_BT}\right)\times{\rm Im}\left[-i\int_0^{\infty} dt e^{i\omega t}\langle[B^-(t), B^+(0)]\rangle\right]. \quad \text{(A3)}$$

As a result, the relaxation time is given by

$$1/T_1 = \frac{(g\mu_B)^2}{2\hbar^2}\coth\left(\frac{\hbar\omega}{2k_BT}\right){\rm Im}\left[\mathcal{C}^R_{B^-B^+}(\omega)\right], \quad \text{(A4)}$$

where we denote $\mathcal{C}^R_{AB}(\omega) = -i\int_0^{\infty} dt e^{i\omega t}\langle[A(t), B(0)]\rangle$.

APPENDIX B: WIRE-INDUCED ELECTROMAGNETIC MODES

Here we calculate the electromagnetic modes induced by charge and spin densities in a 1D system. Following the convention in the main text, the wire is aligned in the $\hat{\boldsymbol{x}}$ axis, and $\boldsymbol{r}_\perp = (y, z)$ are the coordinates transverse to the wire. Without loss of generality, we also assume that the probe is in position $\boldsymbol{r} = (0, 0, R)$. In the following sections, we first find the eigenfunctions $G^\mu_m(q, \boldsymbol{r}_\perp, \omega)$ associated to the vector potential

$$A^\mu(\boldsymbol{r}, t) = \frac{1}{\sqrt{L}}\sum_{q\omega m} G^\mu_m(q, \boldsymbol{r}_\perp, \omega)e^{i(qx-\omega t)}\rho_m(q, \omega), \quad \text{(B1)}$$

for charge ($m = e$) and spin ($m = x, y, z$) modes, and then compute $\boldsymbol{H}_m(q, \boldsymbol{r}_\perp, \omega)$ in Eq. (4) by taking the curl of $G^\mu_m(q, \boldsymbol{r}_\perp, \omega)$.

1. Charge-induced electromagnetic modes

The electromagnetic mode associated with the 1D charge density is given by the solution of

$$\left[(\omega/c)^2 - q^2 + \nabla^2_{\boldsymbol{r}_\perp}\right]G^\mu_e(q, \boldsymbol{r}_\perp, \omega) = \delta(\boldsymbol{r}_\perp)d^\mu(q, \omega), \qquad d^\mu(q, \omega) = (1, \omega/q, 0, 0). \quad \text{(B2)}$$

Here, we focus on evanescent wave solutions, $q \geqslant \omega/c$, because typical excitation wavevectors q are on the order of $q \sim \omega/v_F$, with $v_F \ll c$. The 4-vector $d^\mu(q, \omega)$ originates the continuity equation, $\partial_t\rho_e + \partial_z j_e = 0$. The explicit solution of Eq. (B2) is

$$G^\mu_e(q, \boldsymbol{r}_\perp, \omega) = -[d^\mu(q, \omega)/2\pi]K_0(\lambda|\boldsymbol{r}_\perp|), \quad \text{(B3)}$$

where K_n denotes the nth modified Bessel function of the second kind, and $\lambda = \sqrt{q^2 - (\omega/c)^2}$. The magnetic field at the position of the probe $\boldsymbol{r} = (0, 0, R)$ is given by Eq. (5), where $\boldsymbol{H}_m(q, \boldsymbol{r}_\perp, \omega)$ is found by taking the curl of Eq. (B2).

2. Spin-induced electromagnetic modes

Similarly, the electromagnetic modes corresponding to the spin source are given by the solution of

$$[(\omega/c)^2 - q^2 + \nabla^2_{\boldsymbol{r}_\perp}]G^\mu_m(q, \boldsymbol{r}_\perp, \omega) = [0, \boldsymbol{\nabla}\times(\delta(\boldsymbol{r}_\perp)\hat{\boldsymbol{e}}_m)], \quad \text{(B4)}$$

where $\boldsymbol{\nabla}$ reads $\boldsymbol{\nabla} = (iq, \partial_y, \partial_z)$. The explicit solutions of Eq. (B4) are

$$G_x^\mu = \frac{1}{2\pi}\begin{pmatrix} 0 \\ 0 \\ \lambda K_1(\lambda r)\sin\theta \\ -\lambda K_1(\lambda r)\cos\theta \end{pmatrix},$$

$$G_y^\mu = \frac{1}{2\pi}\begin{pmatrix} 0 \\ -\lambda K_1(\lambda r)\sin\theta \\ 0 \\ iqK_0(\lambda r) \end{pmatrix},$$

$$G_z^\mu = \frac{1}{2\pi}\begin{pmatrix} 0 \\ -\lambda K_1(\lambda r)\cos\theta \\ -iqK_0(\lambda r) \\ 0 \end{pmatrix}. \tag{B5}$$

By taking the curl of Eq. (B5) and using $\omega/c \ll q$, we find $\boldsymbol{H}_m(q, \boldsymbol{r}_\perp, \omega)$ at $\boldsymbol{r} = (0, 0, R)$ given by Eq. (6).

APPENDIX C: RELAXATION TIME AND DENSITY-DENSITY CORRELATORS

The relaxation rate can be obtained from inserting the magnetic field induced by charge [Eq. (5)] and spin [Eq. (6)] modes into Eq. (3). To measure charge-induced fluctuations, we assume that the probe is polarized in the $\hat{z}$ direction, such that $\delta B^\pm = \delta B^x \pm i\delta B^y$ (see Fig. 1). As a result, we find that $\langle[\delta B^-, \delta B^+]\rangle = \sum_q F_e(q)\langle[\rho_e, \rho_e]\rangle$, where

$$F_e(q) = \left(\frac{\mu_0 e\omega}{2\pi}\right)^2 K_1^2(qR). \tag{C1}$$

For spin modes, we assume that the probe is polarized in the $\hat{y}$ direction, such that $\delta B^\pm = \delta B_z \pm i\delta B_x$. For system with an SU(2) spin degree of freedom, we find that $\langle[\delta B^-, \delta B^+]\rangle = \sum_q F_\sigma(q)\langle[\rho_\sigma, \rho_\sigma]\rangle$, where

$$F_\sigma(q) = \left(\frac{\mu_0 g_\sigma \mu_B q}{4\pi}\right)^2 \left[(K_0 - K_2)^2 + 8K_1^2 + 4K_0^2\right], \tag{C2}$$

where we used the fact that $\langle\rho_x\rho_x\rangle = \langle\rho_z\rho_z\rangle = \langle\rho_\sigma\rho_\sigma\rangle$. In the limit $qR \lesssim 1$, we find that F_σ is dominated by $F_\sigma \approx (\frac{\mu_0 g_\sigma \mu_B q}{4\pi})^2 K_2^2(qR)$. Instead, for spin-polarized systems with polarization angles $\rho_x = \rho_\sigma \cos\theta$, $\rho_y = \rho_\sigma \sin\theta\sin\varphi$, and $\rho_z = \rho_\sigma \sin\theta\cos\varphi$, we find $\langle[\delta B^-, \delta B^+]\rangle = \sum_q F_\sigma(q)\langle[\rho_\sigma, \rho_\sigma]\rangle$, where

$$F_\sigma(q) = \left(\frac{\mu_0 g_\sigma \mu_B q^2}{4\pi}\right)^2 \Big\{4(K_0 + K_1)^2\cos^2\theta + \left[(K_0 - K_2)^2 + 4K_1^2\right]\sin^2\theta\cos^2\varphi\Big\}. \tag{C3}$$

Here we assume that the direction of polarization has some finite components in the direction transverse to the wire [otherwise, magnetic noise will be a factor $(qR)^2$ smaller for distances $R < 1/q$]. In the limit $qR \lesssim 1$, we find that F_σ is dominated by $F_\sigma \approx (\frac{\mu_0 g_\sigma \mu_B q}{4\pi})^2 K_2^2(qR)\cos^2\theta\sin^2\varphi$.

APPENDIX D: MEMORY FUNCTION FOR DISORDER

For the SU(2) case, the memory functions are defined in terms of the retarded correlator $\mathcal{C}^{\rm R}_{f_m f_m}(q, \omega)$, where $f_m(x) = [\Pi_m(x), \int dx' \mathcal{H}_{\rm dis}(x')]$ captures the momentum relaxation rate of Π_m. Explicitly, $f_m(x)$ takes values $f_m(x) = (2v_m\mathcal{K}_m/a)u(x)e^{i\sqrt{2}\phi_e(x)}\cos[\sqrt{2}\phi_\sigma(x)] + \text{H.c.}$ Calculations of correlations functions where the field $\phi_m(x)$ appears in the exponent is straightforward but tedious. A detailed step-by-step procedure is discussed in Appendix C of Ref. [3]. Using $\langle u(x)\bar{u}(x')\rangle = D\delta(x - x')$, the correlation function can be expressed as in Eq. (28) with parameters

$$\begin{aligned}\Gamma_m &= (2\pi)^{\mathcal{K}_t+1} D\mathcal{K}_m^2 v_m^{\mathcal{K}_t}/v_e^{\mathcal{K}_e} v_\sigma^{\mathcal{K}_\sigma}, \\ \alpha_m &= \mathcal{K}_t - 2, \\ \mathcal{F}_m(x) &= \sin(\pi\mathcal{K}_t/2) \\ &\quad\times \frac{B(\mathcal{K}_t/2 - ix, 1 - \mathcal{K}_t) - B(\mathcal{K}_t/2, 1 - \mathcal{K}_t)}{x},\end{aligned} \tag{D1}$$

where $B(x, y)$ is the Beta function and $\mathcal{K}_t = \mathcal{K}_e + \mathcal{K}_\sigma$. For repulsive interactions, our numerical estimates show that that the dimensionless function $\mathcal{F}_m(x)$ can be approximated as $\mathcal{F}_m(x \lesssim 1) \approx \beta i$, where $1 \lesssim \beta \lesssim 5$ for a wide range of $\mathcal{K}_{e,\sigma}$ and x values.

The same procedure holds for the scattering potential in Eq. (30), where $f(x) = (v_e\mathcal{K}_e/a)u_n(x)e^{i2n\phi_e(x)} + \text{H.c.}$ Assuming an uncorrelated scattering potential, $\langle u_n(x)u_n(x')\rangle = D_n\delta(x - x')$ leads to Eq. (28) with parameters

$$\begin{aligned}\Gamma_n &= \frac{2^{2n\mathcal{K}_e - 2}}{\pi}\frac{D_n\mathcal{K}_e}{v_e}, \quad \alpha_n = 2n\mathcal{K}_e - 2, \\ \mathcal{F}_n(x) &= \sin(\pi\mathcal{K}_e)\frac{B(\mathcal{K}_e - ix, 1 - 2\mathcal{K}_e) - B(\mathcal{K}_e, 1 - 2\mathcal{K}_e)}{x}.\end{aligned} \tag{D2}$$

For $n = 1$ and repulsive interactions, our numerical estimates show that that the function $\mathcal{F}_n(x \lesssim 1)$ can be approximated as $f_1(x) \approx \beta_1 i$, where $1 \lesssim \beta_1 \lesssim 3$ for a wide range of $\mathcal{K}_e$ and x values. For $n = 2$, the function $\mathcal{F}_n(x)$ can be approximated as $\mathcal{F}_2(x \lesssim 1) \approx \beta_2 i$, where $0.1 \lesssim \beta_2 \lesssim 1$ for a wide range of $\mathcal{K}_e$ and x values.

[1] J. Voit, One-dimensional fermi liquids, Rep. Prog. Phys. **58**, 977 (1995).

[2] J. von Delft and H. Schoeller, Bosonization for beginners — refermionization for experts, Ann. Phys. **7**, 225 (1998).

[3] T. Giamarchi, *Quantum Physics in One Dimension* (Clarendon Press, Oxford, 2003).

[4] Y. K. Kato, R. C. Myers, A. C. Gossard, and D. D. Awschalom, Observation of the spin hall effect in semiconductors, Science **306**, 1910 (2004).

[5] J. Wunderlich, B. Kaestner, J. Sinova, and T. Jungwirth, Experimental Observation of the Spin-Hall Effect in a Two-Dimensional Spin-Orbit Coupled Semiconductor System, Phys. Rev. Lett. **94**, 047204 (2005).

[6] V. Sih, R. C. Myers, Y. K. Kato, W. H. Lau, A. C. Gossard, and D. D. Awschalom, Spatial imaging of the spin hall effect and current-induced polarization in two-dimensional electron gases, Nat. Phys. **1**, 31 (2005).

[7] M. König, S. Wiedmann, C. Brüne, A. Roth, H. Buhmann, L. W. Molenkamp, X.-L. Qi, and S.-C. Zhang, Quantum spin hall insulator state in hgte quantum wells, Science **318**, 766 (2007).

[8] L. Rondin, J.-P. Tetienne, T. Hingant, J.-F. Roch, P. Maletinsky, and V. Jacques, Magnetometry with nitrogen-vacancy defects in diamond, Rep. Prog. Phys. **77**, 056503 (2014).

[9] J. M. Taylor, P. Cappellaro, L. Childress, L. Jiang, D. Budker, P. R. Hemmer, A. Yacoby, R. Walsworth, and M. D. Lukin, High-sensitivity diamond magnetometer with nanoscale resolution, Nat. Phys. **4**, 810 (2008).

[10] S. Kolkowitz, A. Safira, A. A. High, R. C. Devlin, S. Choi, Q. P. Unterreithmeier, D. Patterson, A. S. Zibrov, V. E. Manucharyan, H. Park, and M. D. Lukin, Probing johnson noise and ballistic transport in normal metals with a single-spin qubit, Science **347**, 1129 (2015).

[11] T. van der Sar, F. Casola, R. Walsworth, and A. Yacoby, Nanometre-scale probing of spin waves using single electron spins, Nat. Commun. **6**, 7886 (2015).

[12] H. J. Mamin, M. Kim, M. H. Sherwood, C. T. Rettner, K. Ohno, D. D. Awschalom, and D. Rugar, Nanoscale nuclear magnetic resonance with a nitrogen-vacancy spin sensor, Science **339**, 557 (2013).

[13] C. Du, T. van der Sar, T. X. Zhou, P. Upadhyaya, F. Casola, H. Zhang, M. C. Onbasli, C. A. Ross, R. L. Walsworth, Y. Tserkovnyak, and A. Yacoby, Control and local measurement of the spin chemical potential in a magnetic insulator, Science **357**, 195 (2017).

[14] P. Glover and S. P. Mansfield, Limits to magnetic resonance microscopy, Rep. Prog. Phys. **65**, 1489 (2002).

[15] E. M. Spanton, K. C. Nowack, L. Du, G. Sullivan, and R.-R. Du, and K. A. Moler, Images of Edge Current in InAs/GaSb Quantum Wells, Phys. Rev. Lett. **113**, 026804 (2014).

[16] K. Agarwal, R. Schmidt, B. Halperin, V. Oganesyan, G. Zaránd, M. D. Lukin, and E. Demler, Magnetic noise spectroscopy as a probe of local electronic correlations in two-dimensional systems, Phys. Rev. B **95**, 155107 (2017).

[17] B. J. Maertz, A. P. Wijnheijmer, G. D. Fuchs, M. E. Nowakowski, and D. D. Awschalom, Vector magnetic field microscopy using nitrogen vacancy centers in diamond, App. Phys. Lett. **96**, 092504 (2010).

[18] C. Kim, A. Y. Matsuura, Z.-X. Shen, N. Motoyama, H. Eisaki, S. Uchida, T. Tohyama, and S. Maekawa, Observation of Spin-Charge Separation in One-Dimensional $SrCuo_2$, Phys. Rev. Lett. **77**, 4054 (1996).

[19] R. Neudert, M. Knupfer, M. S. Golden, J. Fink, W. Stephan, K. Penc, N. Motoyama, H. Eisaki, and S. Uchida, Manifestation of Spin-Charge Separation in the Dynamic Dielectric Response of One-Dimensional $sr_2Cu\,O_3$, Phys. Rev. Lett. **81**, 657 (1998).

[20] P. Segovia, D. Purdie, M. Hengsberger, and Y. Baer, Observation of spin and charge collective modes in one-dimensional metallic chains, Nature (London) **402**, 504 (1999).

[21] O. M. Auslaender, H. Steinberg, A. Yacoby, Y. Tserkovnyak, B. I. Halperin, K. W. Baldwin, L. N. Pfeiffer, and K. W. West, Spin-charge separation and localization in one dimension, Science **308**, 88 (2005).

[22] Y. Jompol, C. J. B. Ford, J. P. Griffiths, I. Farrer, G. A. C. Jones, D. Anderson, D. A. Ritchie, T. W. Silk, and A. J. Schofield, Probing spin-charge separation in a tomonaga-luttinger liquid, Science **325**, 597 (2009).

[23] C. L. Degen, F. Reinhard, and P. Cappellaro, Quantum Sensing. Rev. Mod. Phys. **89**, 035002 (2017).

[24] J. M. Luttinger, An exactly soluble model of a many-fermion system, J. Math. Phys. **4**, 1154 (1963).

[25] D. C. Mattis and E. H. Lieb, Exact solution of a Many-Fermion system and its associated boson field, J. Math. Phys. **6**, 304 (1965).

[26] F. D. M. Haldane, Effective Harmonic-Fluid Approach to Low-Energy Properties of One-Dimensional Quantum Fluids, Phys. Rev. Lett. **47**, 1840 (1981).

[27] Y.-W. Son, M. L. Cohen, and S. G. Louie, Half-metallic graphene nanoribbons, Nature (London) **444**, 347 (2006).

[28] C.-K. Wang and K.-F. Berggren, Spin splitting of subbands in quasi-one-dimensional electron quantum channels, Phys. Rev. B **54**, R14257 (1996).

[29] C. L. Kane and E. J. Mele, Quantum Spin Hall Effect in Graphene, Phys. Rev. Lett. **95**, 226801 (2005).

[30] J. Maciejko, C. Liu, Y. Oreg, X.-L. Qi, C. Wu, and S.-C. Zhang, Kondo Effect in the Helical Edge Liquid of the Quantum Spin Hall State, Phys. Rev. Lett. **102**, 256803 (2009).

[31] A. Ström, H. Johannesson, and G. I. Japaridze, Edge Dynamics in a Quantum Spin Hall State: Effects from Rashba Spin-Orbit Interaction, Phys. Rev. Lett. **104**, 256804 (2010).

[32] Y. Tanaka, A. Furusaki, and K. A. Matveev, Conductance of a Helical Edge Liquid Coupled to a Magnetic Impurity, Phys. Rev. Lett. **106**, 236402 (2011).

[33] T. L. Schmidt, S. Rachel, F. von Oppen, and L. I. Glazman, Inelastic Electron Backscattering in a Generic Helical Edge Channel, Phys. Rev. Lett. **108**, 156402 (2012).

[34] J. I. Väyrynen, M. Goldstein, and L. I. Glazman, Helical Edge Resistance Introduced by Charge Puddles, Phys. Rev. Lett. **110**, 216402 (2013).

[35] J. I. Väyrynen, M. Goldstein, Y. Gefen, and L. I. Glazman, Resistance of helical edges formed in a semiconductor heterostructure, Phys. Rev. B **90**, 115309 (2014).

[36] G. S. Agarwal, Quantum electrodynamics in the presence of dielectrics and conductors. i. electromagnetic-field response functions and black-body fluctuations in finite geometries, Phys. Rev. A **11**, 230 (1975).

[37] C. Henkel, S. Pötting, and M. Wilkens, Loss and heating of particles in small and noisy traps, Appl. Phys. B **69**, 379 (1999).

[38] A. I. Volokitin and B. N. J. Persson, Near-field radiative heat transfer and noncontact friction, Rev. Mod. Phys. **79**, 1291 (2007).

[39] L. S. Langsjoen, A. Poudel, M. G. Vavilov, and R. Joynt, Qubit relaxation from evanescent-wave johnson noise, Phys. Rev. A **86**, 010301 (2012).

[40] A. Poudel, L. S. Langsjoen, M. G. Vavilov, and R. Joynt, Relaxation in quantum dots due to evanescent-wave johnson noise, Phys. Rev. B **87**, 045301 (2013).

[41] J. Korringa. Nuclear magnetic relaxation and resonance line shift in metals, Physica **16**, 601 (1950).

[42] A. Jarmola, V. M. Acosta, K. Jensen, S. Chemerisov, and D. Budker, Temperature- and Magnetic-Field-Dependent Longitudinal Spin Relaxation in Nitrogen-Vacancy Ensembles in Diamond, Phys. Rev. Lett. **108**, 197601 (2012).

[43] C. Xu and J. E. Moore, Stability of the quantum spin hall effect: Effects of interactions, disorder, and Z_2 topology, Phys. Rev. B **73**, 045322 (2006).

[44] H. Fukuyama and P. A. Lee, Dynamics of the charge-density wave. I. impurity pinning in a single chain, Phys. Rev. B **17**, 535 (1978).

[45] T. Giamarchi and P. Le Doussal, Variational theory of elastic manifolds with correlated disorder and localization of interacting quantum particles, Phys. Rev. B **53**, 15206 (1996).

[46] W. Götze and P. Wölfle, Homogeneous dynamical conductivity of simple metals, Phys. Rev. B **6**, 1226 (1972).

[47] T. Giamarchi and H. J. Schulz, Anderson localization and interactions in one-dimensional metals, Phys. Rev. B **37**, 325 (1988).

[48] T. Giamarchi, Umklapp process and resistivity in one-dimensional fermion systems, Phys. Rev. B **44**, 2905 (1991).

[49] A. Garg, D. Rasch, E. Shimshoni, and A. Rosch, Large Violation of the Wiedemann-Franz Law in Luttinger Liquids, Phys. Rev. Lett. **103**, 096402 (2009).

[50] U. Balucani, M. Howard Lee, and V. Tognetti, Dynamical correlations, Phys. Rep. **373**, 409 (2003).

[51] H. M. Transport, C. Motion, and B. Motion, Prog. Theor. Phys. **33**, 423 (1965).

[52] T. Nattermann, T. Giamarchi, and P. Le Doussal, Variable-Range Hopping and Quantum Creep in One Dimension, Phys. Rev. Lett. **91**, 056603 (2003).

[53] L. F. Cugliandolo, T. Giamarchi, and P. Le Doussal, Dynamic Compressibility and Aging in Wigner Crystals and Quantum Glasses, Phys. Rev. Lett. **96**, 217203 (2006).

[54] R. N. Bhatt and D. S. Fisher, Absence of Spin Diffusion in Most Random Lattices, Phys. Rev. Lett. **68**, 3072 (1992).

[55] C. L. Kane and M. P. A. Fisher, Transmission through barriers and resonant tunneling in an interacting one-dimensional electron gas, Phys. Rev. B **46**, 15233 (1992).

[56] C. L. Kane and M. P. A. Fisher, Transport in a One-Channel Luttinger Liquid, Phys. Rev. Lett. **68**, 1220 (1992).

[57] K. J. Thomas, J. T. Nicholls, M. Y. Simmons, M. Pepper, D. R. Mace, and D. A. Ritchie, Possible Spin Polarization in a One-Dimensional Electron Gas, Phys. Rev. Lett. **77**, 135 (1996).

[58] A. Yacoby, H. L. Stormer, N. S. Wingreen, L. N. Pfeiffer, K. W. Baldwin, and K. W. West, Nonuniversal Conductance Quantization in Quantum Wires, Phys. Rev. Lett. **77**, 4612 (1996).

[59] A. P. Micolich, What lurks below the last plateau: experimental studies of the $0.7 \times 2e^2/h$ conductance anomaly in one-dimensional systems, J. Phys.: Condens. Matter **23**, 443201 (2011).

[60] V. A. Volkov and S. A. Mikhailov, Edge magnetoplasmons: low frequency weakly damped excitations in inhomogeneous two-dimensional electron systems, Sov. Phys. JETP **67**, 1639 (1988).

[61] M. S. Grinolds, S. Hong, P. Maletinsky, L. Luan, M. D. Lukin, R. L. Walsworth, and A. Yacoby, Nanoscale magnetic imaging of a single electron spin under ambient conditions, Nat. Phys. **9**, 215 (2013).

[62] J.-P. Tetienne, T. Hingant, L. J. Martínez, S. Rohart, A. Thiaville, L. Herrera Diez, K. Garcia, J.-P. Adam, J.-V. Kim, J.-F. Roch, I. M. Miron, G. Gaudin, L. Vila, B. Ocker, D. Ravelosona, and V. Jacques, The nature of domain walls in ultrathin ferromagnets revealed by scanning nanomagnetometry, Nat. Commun. **6**, 6733 (2015).